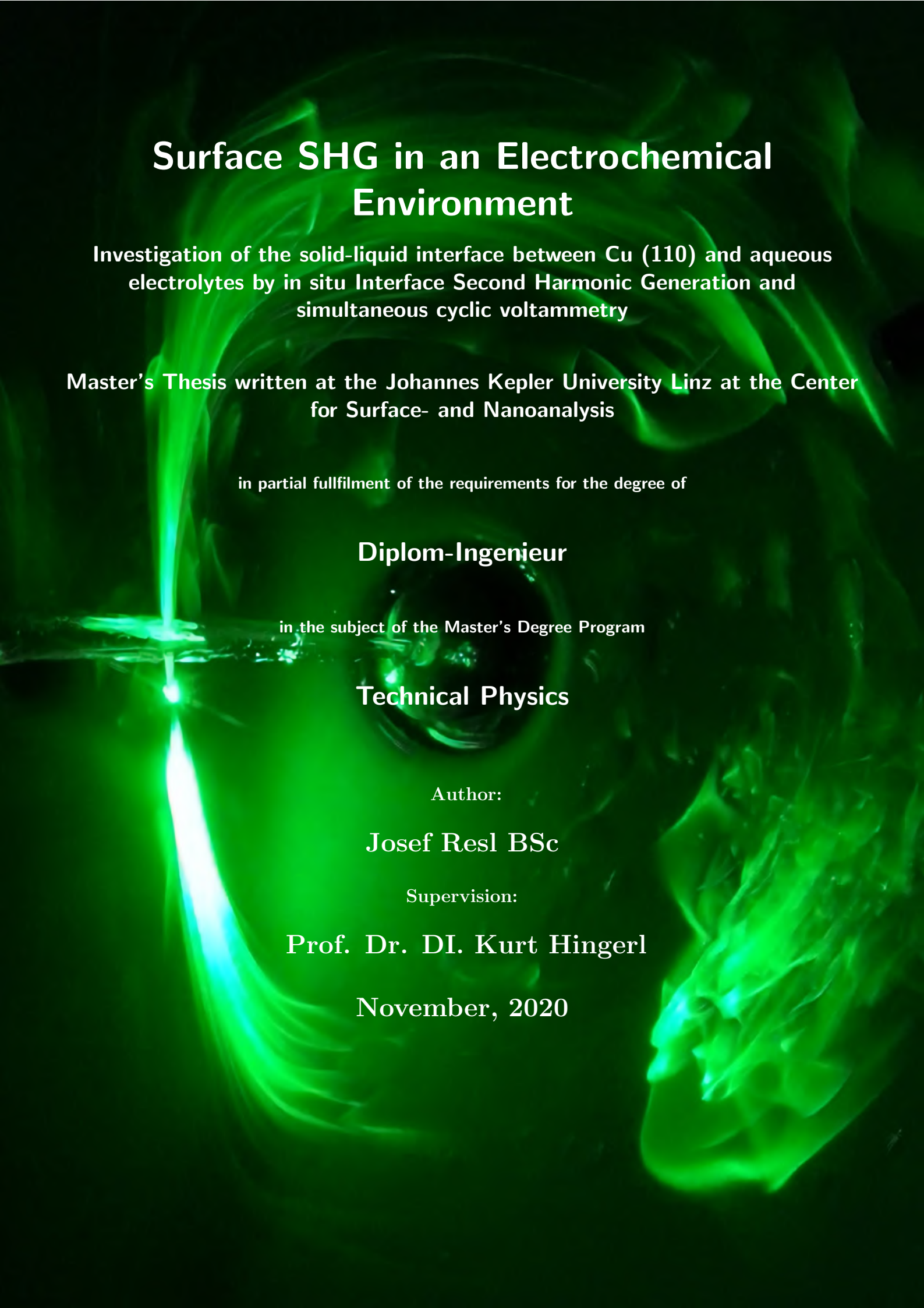

Surface SHG in an Electrochemical Environment

Investigation of the solid-liquid interface between Cu (110) and aqueous electrolytes by in situ Interface Second Harmonic Generation and simultaneous cyclic voltammetry

Master's Thesis written at the Johannes Kepler University Linz at the Center for Surface- and Nanoanalysis

in partial fullfilment of the requirements for the degree of

Diplom-Ingenieur

in the subject of the Master's Degree Program

Technical Physics

Author:

Josef Resl BSc

Supervision:

Prof. Dr. DI. Kurt Hingerl

November, 2020

Acknowledgements

First and foremost I want to thank:

- Professor Dr. DI. Kurt Hingerl for believing in me and providing a suitable work environment as well as being a laid back supervisor.
- Dr. Christoph Cobet for being a hands-off supervisor with deep knowledge in his field of research.
- Saul Vazquez Miranda, now PhD, who taught me with patience the very basic basics of his lab
- Dr. Eric Eugenio López, who helped me with the experiments and who did a lot of the cleaning and assembly procedures regarding the electrochemical equipment.
- AC2T research GmbH for providing financial support as well as the opportunity to study some of the interface properties of lubrication films and metals.
- my parents Karl and Karoline Resl for supporting me until well into adulthood and for encouraging some modes of critical thinking
- my girlfriend Elisabeth Veronika Matzenberger, who always supported me as much as she could since we met in 2008.
- her mother Margit Matzenberger as well as her father Christian Matzenberger who both helped me in many ways.
- Irene Hofbauer, a very close friend of the Margit Matzenberger, who supported me also

Further thanks go to:

- my friends and colleagues from BRG Kirchdorf, Michael Haslecker, Christoph Colak and Daniel Kreuzeder who all went also to JKU to study mathematics or physics.
- my school teacher in elementary school Peter Paul Lintner, who sent me to BRG Kirchdorf for secondary education. He was a very awesome teacher as well, who played the electric guitar and rehearsed and performed a Kasperltheater with us. He did some cool science experiments too. After he showed us a simple electromagnet using a nail, some wire and a battery, I built several of them at home, because I was quite fascinated.
- my physics teacher at the BRG Kirchdorf Mag. Gunther Pickhart, who was always cheerful and very engaged and working hard for his students
- my math teacher at the BRG Kirchdorf Mag. Johann Karl, who always put a strong emphasis on deep understanding and thinking about mathematics as well as teaching me and my colleagues the card game Tarock
- my chemistry teacher at the BRG Kirchdorf, who was a slight pyromaniac and who kept me interested in chemistry

Finally, I want to thank:

- my blind dog Strolchi for our daily walks and for being a good boy and an inspiration since the autumn of 2018, when he unexpectedly arrived.

Abstract

In this thesis, the (110) surface of monocrystalline copper is investigated. This is done via optical and electrochemical methods. More specifically, the surface properties of the copper surface are examined when it is in contact with highly diluted HCl. To examine the electrochemical properties of the system, cyclic voltammetry is used. Cyclic voltammetry helps to detect the potential regions, where adsorption, desorption, hydrogen evolution and copper dissolution take place. In addition, it is very useful to determine, if the sample is clean enough. Optical methods (which are most of the time indirect methods), can give more "direct" answers about the state of the surface than cyclic voltammetry, where the sum of several processes is investigated. The optical method of choice is second harmonics generation at the reflection at the Cu/electrolyte interface. This method has the potential to be very surface sensitive due to symmetry reasons. The work done in this thesis is to a large part the conceptual design of the experimental setup (for simultaneous measurements with both methods), as well as the assembly and initial cleaning procedures that are necessary to start experiments. Furthermore, there has been done a fair amount of troubleshooting in the optical, chemical, mechanical and computer science sense. The main result is that Cl adsorption decreases the SHG intensity for p-polarized input and output. Besides, the measurement(s) shown in this thesis, indicate that, indeed, there is a large sensitivity to surface changes with the second harmonics intensity, even at an unfavorable wavelength. Especially, the cyclic nature of the potential scans can has been exploited to increase the effective sensitivity of this method. In addition, a simple (novel) quasi-normalization procedure, which is free of singularities is employed to further reign in the noise in the system.

Contents

1 Introduction

1.1 Personal Motivation

After my bachelors's thesis, which was basically a X-ray diffraction related software project, I wanted to do something more hands-on in my master's thesis because I really like experiments. If one would ask my parents, they would have some memorable stories to tell, which also involve at least one minor explosion. Anyway, I was looking for an interesting topic for my master's thesis and I had a casual oral exam at Professor Kurt Hingerl's office. During this exam, which mainly aspiring physics teachers take, he asked me: "How would you explain this to a student of yours in the future?". "Not at all, because I am enrolled in technical physics", was my answer. Afterwards, Professor Kurt Hingerl proposed several topics for a prospective master's thesis. Most of it had to do with electron microscopy or wafer bonding. One topic stood out and intrigued me. It was nonlinear optics and was quite interesting. Professor Kurt Hingerl said "Honestly this is somewhat of a "Himmelfahrtskommando" (glory-or-grave-job), but if it works out, great, if not, you explain this in your thesis, negative results are an important part of science". The rest stands in this thesis.

1.2 Scientific Motivation and Goal

Surface science is an ever growing field of interest. Many important properties of materials are determined by surface structure. For example corrosion resistance, tribologic properties or catalytic efficiency and so much more. The surface of a material is more accessible and more complicated in its behaviour than the bulk of a material due to the influence of the environment, symmetry breaking and localized surface states, just to name the more prominent causes.

At ZONA (especially Dr. Christoph Cobet), a lot of investigations into the catalytic efficiency of copper during the hydrogen evolution reaction has been carried out. Especially the role of the adsorption of Cl ions in diluted HCl, was investigated with cyclic voltammetry and ellipsometry simultaneously in an electrochemical cell with transparent windows, which is difficult enough to start with.

The idea for this thesis was to try another optical method that is more surface sensitive than ellipsometry or RAS (Reflectance anisotropy spectroscopy), which, with the right know-how from ZONA is already sub-ML sensitive.

Since the inception of the "Christian Doppler Laboratorium für mikroskopische und spektroskopische Materialcharakterisierung" (head: Assoc. Univ.-Prof. DI Dr. David Stifter), there is a ps - laser with tunable wavelength at the ZONA, which can be tuned from the visible range up to 10 microns in wavelength. With this laser system some research into surface second harmonics generation (such as at the air/Si interface) has been done. The goal for this thesis is to investigate the feasibility of simultaneous cyclic voltammetry and surface SHG measurements at the interface between copper and an electrolyte.

This adds several challenges to an already difficult experiment: Nonlinear optics measurements are heavily impacted by laser intensity fluctuations. The signals generated are very weak and the tools for the analysis of such measurements are nowhere near as well developed as for ellipsometry, which is a much used experimental technique, where a lot of things are available like powerful ellipsometers

completely with a software stack, for the analysis of complex, layered interfaces. Nonetheless, surface SHG has the potential to be extremely surface sensitive due to its nature. Therefore, this thesis will investigate, if this method of surface analysis has any merit.

There are several questions regarding the Cu (110) surface as well:

- is there any correlation between CV and SHG and what is a possible mechanism for that?
- can we learn something about the adsorption process itself?
- has CuCl, which forms on the surface at certain potentials a covalent bond between Cu and Cl or is the bond undirected?
- is the electron spillout at the surface homogeneous or not and what does this mean for the SHG intensity/signal at different polarisations?

2 Metal-Electrolyte Interface

2.1 Copper Surfaces

2.1.1 Copper

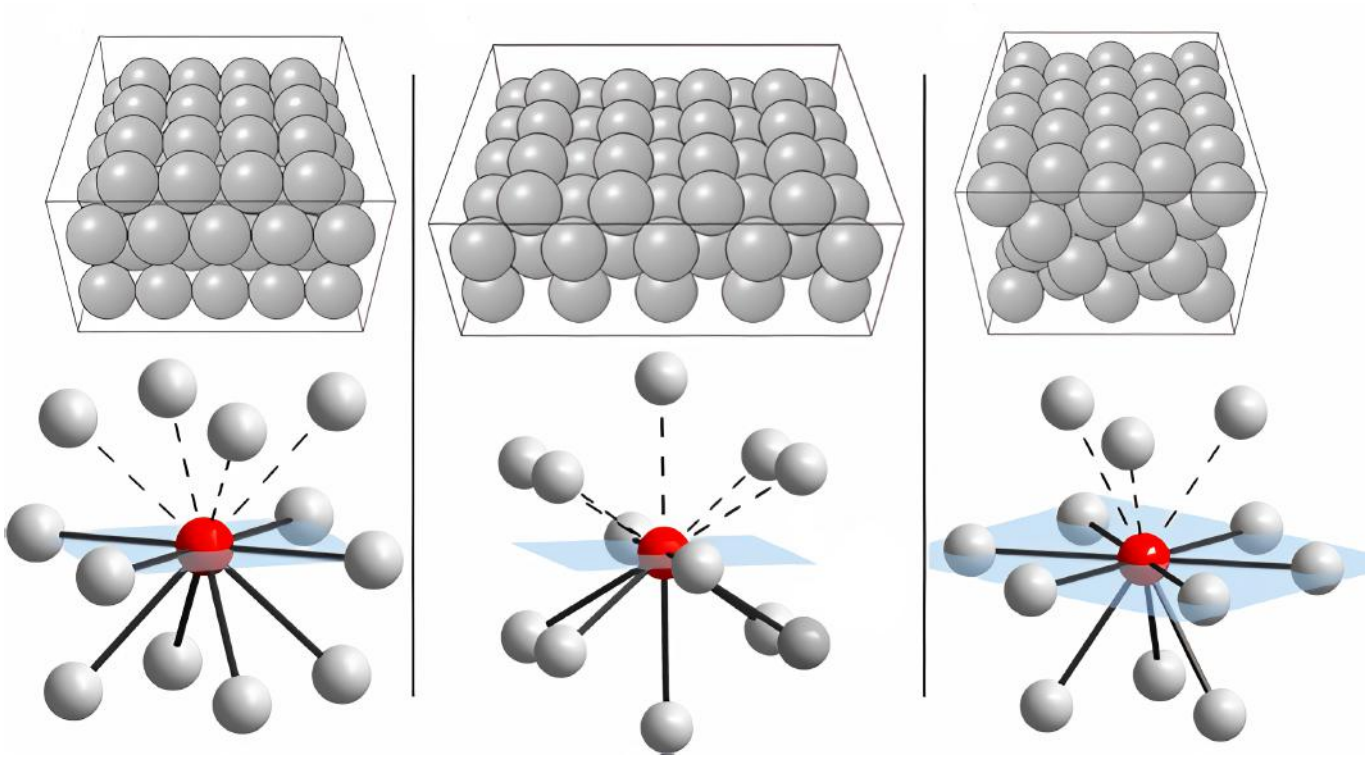

Figure 2.1: Left to right: (100), (110) and (111) surface with nearest neighbours shown below - taken from ref.[8]

The crystal structure of copper is, like many other metals, face-centered cubic. The copper crystal is held together not by covalent bonds but rather by the spherically symmetric 4s electrons of the copper atoms, which give copper its characteristic high ductility and low hardness. Every copper atom contributes its 4s electron to the conduction band, which is an important prerequisite for excellent electrical and thermal conductivity.

2.1.2 Copper(110)

Of the low index surfaces, the (110) surface has the lowest degree of symmetry (rectangular symmetry). In the bulk of the metal every copper atom has 12 nearest neighbours, while at the (110) surface, 5 of them are missing in the topmost layer, so 7 neighbours remain. The topmost atoms are arranged in a rectangular lattice, with the spacing between the atoms being a_{bulk} and $a_{\text{bulk}}/\sqrt{2}$, sans the effects of surface reconstruction, which modify the lattice constant a near the surface. Therefore,

the top layer is arranged in rows, unlike the (111) or the (100) surface. As a result of this, the (110) surface is very open in the sense that, it has a lower density of copper atoms than the (111) or the (100) surface in the topmost layer. This leads to more possible adsorption sites, lower work function and a larger surface free energy. The higher number of broken bonds makes the surface less stable in general, when compared to the (100) and (111) surfaces.

2.2 Electrolyte

Electrolytes in the most general sense are substances, which consist partially of ions, that are free enough to move, such that they can support an electrical current. In our case this is a liquid solvent (ultrapure H_2O) and a solute (HCl) that dissociates into ions:

$$\mathrm{HCl_{(g)} + H_2O_{(l)} \longrightarrow H_3O^+{}_{(aq)} + Cl^-{}_{(aq)}} \tag{2.1}$$

2.2.1 Electrochemical Window

If two conducting electrodes are placed in an aqueous electrolyte, and a voltage is applied, at a specific threshold voltage, electrolysis takes place:

$$\mathrm{2\,H_2O \longrightarrow 2\,H_2 + O_2} \tag{2.2}$$

The base solvent water disintegrates into gaseous hydrogen and oxygen. The hydrogen evolution reaction (HER) takes place at the cathode and is a reduction reaction:

$$\mathrm{2\,H^+{}_{(aq)} + 2\,e^- \longrightarrow 2\,H_{2\,(g)}} \tag{2.3}$$

At the cathode oxygen is produced by the oxidation of water:

$$\mathrm{2\,H_2O_{(l)} \longrightarrow O_{2\,(g)} + 4\,H^+{}_{(aq)} + 4\,e^-} \tag{2.4}$$

The H^+ ions have to diffuse from the cathode to the anode and may attach themselves to water molecules to form hydronium ions along the way: $\mathrm{H^+ + H_2O \longleftrightarrow H_3O^+}$.

Both reactions above are balanced with acid. The reaction only occurs above a certain voltage threshold, which depends on pH and the material of the electrodes as well as the solutes in the water.

2.3 Charged Layers at the Electrolyte-Electrode Interface

At the interface of the copper electrode and the electrolyte, several (charged) adlayers form (see Fig. 2.2). Those layers can change through sorption processes, which are heavily influenced by the electronic charge, that the metal surface holds. This charge depends on the potential difference across the interface in a nontrivial way, as the electrons are also influenced by the (charged) adlayers themselves.

2.3.1 Inner Helmholtz Layer and Specific Adsorption

Ions from the electrolyte solution can adsorb to the surface like Cl^- and H^+. To adsorb directly (specific adsorption) to the copper surface, the anion has to move from the bulk of the electrolyte to the surface of the electrode. Then, it is necessary to break the solvation shell of the anion, which of course requires energy. Besides, the water molecules at the surface have to desorb to create space

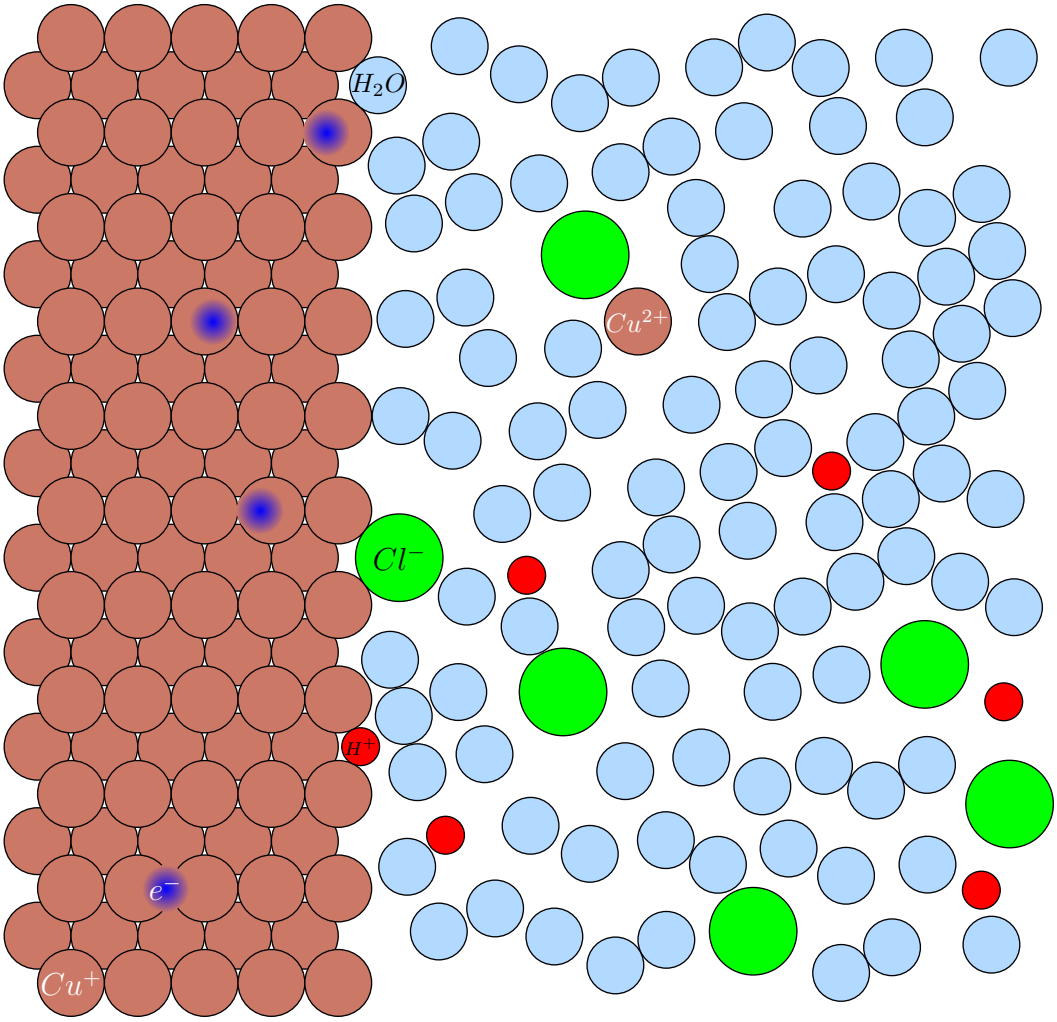

Figure 2.2: Metal-electrolyte interface: Copper crystal is on the left, water molecules are light blue and Cl ions are green, H^+ ions are red and electrons are blue with fuzzy edges

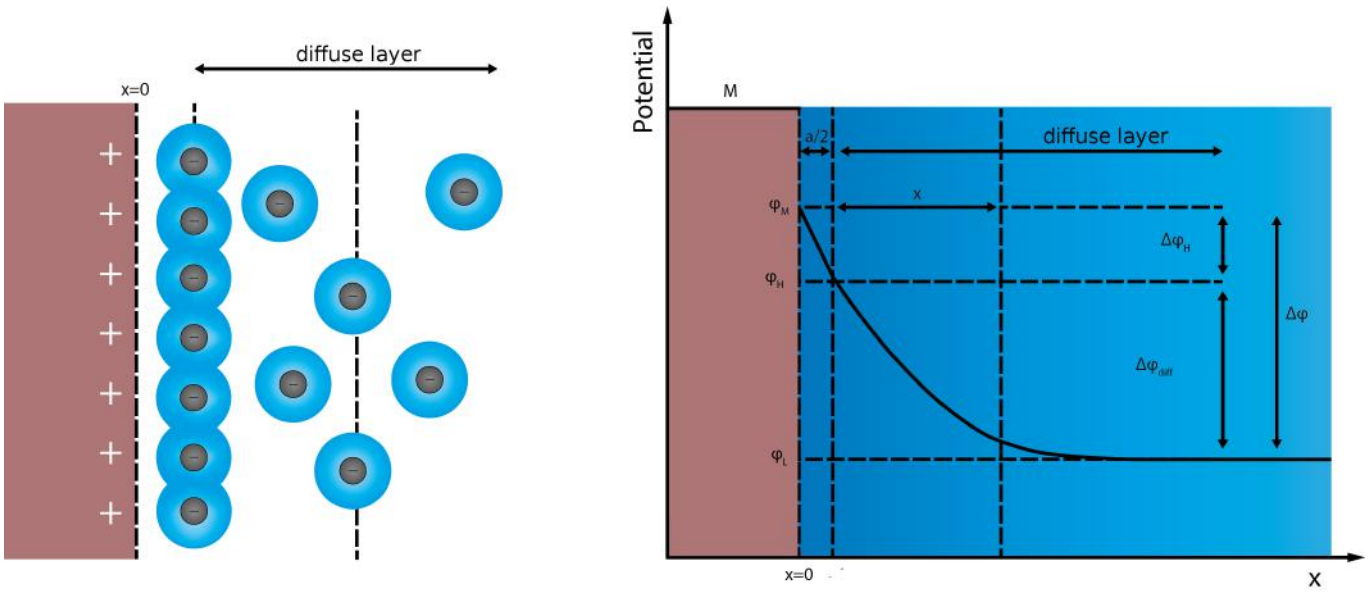

Figure 2.3: The potential φ in the electrolyte drops linearly in the rigid Helmholtz layer and quasi-exponentially in the diffuse layer. Image taken from ref.[12] with some modifications.

for the anion. After that the anion comes into direct contact with the copper surface and is now specifically adsorbed. If there is more than one anion adsorbed at the (flat) surface, then they form an adsorbate layer, if the number of adsorbed anions is comparable to the number of surface atoms. This layer is called the inner Helmholtz layer. The anions in the layer repel each other due to electrostatic repulsion and interact attractively with the electronic charge of the electrode. In addition, they are attracted to their image charges in the electrode. The inner Helmholtz layer can be seen as a parallel-plate capacitor with constant electric field between the plates and linear variation of the potential from plate to plate.

Whether adsorption or desorption of the ions takes place depends on the potential at the surface. This potential influences the electronic surface charge, which interacts with the ions in the solution (described above). In the same way the rate of adsorption/desorption depends on the surface potential. Through such sorption processes the ionic charge of the surface is altered via charging or discharging.

2.3.2 Unspecific Adsorption and Diffuse Layer

Similarly, ions can adsorb to the electrode surface with their hydration shells intact, which results in a weaker bond, this is the outer Helmholtz layer. Then there is a diffuse layer (Gouy-Chapman model), which consists of ions attracted by the electrical field near the surface of the electrode. Their concentration is higher than in the bulk of the electrolyte and they weaken the electric field in the direction of the bulk. They move freely near the electrode surface and are not adsorbed.

2.3.3 Cl Adsorption on Cu and CV Current

When one chloride anion adsorbs on the surface, it reduces the surface electron excess Γ_e by approximately one electron charge[3], which leads to a measurable current, when many ions adsorb at the same time. This current is proportional to the adsorption rate. The surface electron excess is the leaking out of electrons from the metal. This can be understood with the jellium model. The metal consists of cations that make up the crystal structure and free electrons. Those free electrons are held captive by the Coulomb well of those cations. Due to quantum mechanics, the electrons can leak out a little bit (exponentially decreasing probability of finding electrons with increasing distance to the surface), as the Coulomb well is not an infinitely high energy barrier. So there is an excess of electrons near the surface. This region can extend up to 10 nm distance from the surface, but is usually only a few Å wide.

2.3.4 Adsorption Isothermes

Frumkin Isotherm

The surface coverage of the adsorbed anions can be described in a idealized, phenomenological manner by the Frumkin isotherm:

$$\Delta G_{ad} - q_e U + \frac{k_B T}{n} \ln(\frac{\theta}{1-\theta}) + w\theta = 0 \tag{2.5}$$

Here, θ is the surface coverage of the species (Cl^-) of interest. The surface coverage is the ratio of adsorbed ions to the number of available adsorption sites: $\theta = N_{ads}/N_{sites}$. With k_B the Boltzmann constant is denoted and T is the absolute temperature. Further, ΔG_{ad} is the change in the Gibbs free energy when specific adsorption occurs: $G_{ad} - G_{sol}$. The charge number of the active ion species is n.

Finally, w is a factor that represents the adsorbate-adsorbate interaction. For Cl^- anions, this interaction is expected to be repulsive due to the Coulomb interaction. If the adsorbate-adsorbate interaction enhances adsorption, w is negative. If the adsorbate-adsorbate interaction slows down the adsorption process , w is positive. And finally when there is no (effective) adsorbate-adsorbate interaction, then w is zero. And the derivative of this isotherm is:

$$\frac{d\theta}{dU} = \frac{-q_e n\theta(\theta-1)}{k_B T - nw\theta(\theta-1)} \tag{2.6}$$

For $w = 0$, we can calculate θ explicitly:

$$\theta(U) = \frac{1}{e^{\frac{n(-q_e U + \Delta G_{ad})}{k_B T}} + 1} \tag{2.7}$$

Tempkin Isotherm

The Tempkin isotherm is a linearised form of the Frumkin isotherm which can be used when the interaction between the adsorbed ions is weak ($|w|$ is small) or when the surface coverage θ is small.

We take the Frumkin isotherm and set $n = 1$ (for Cl ions) and divide by $k_B T$:

$$\frac{\Delta G_{ad} - q_e U}{k_B T} + \ln(\frac{\theta}{1-\theta}) + \frac{w\theta}{k_B T} = 0 \tag{2.8}$$

Now, we apply the exponential function on both sides and simplify:

$$e^{\frac{\Delta G_{ad} - q_e U}{k_B T}} \frac{\theta}{1-\theta}\, e^{\frac{w\theta}{k_B T}} = 1 \tag{2.9}$$

After that we linearise $e^{\frac{w\theta}{k_B T}}$ for small arguments and we get:

$$e^{\frac{\Delta G_{ad} - q_e U}{k_B T}} \frac{\theta}{1-\theta}(1 + \frac{w\theta}{k_B T}) = 1 \tag{2.10}$$

This is the Tempkin isotherm and it can be brought back into the logarithm form:

$$\Delta G_{ad} - q_e U + k_B T \ln(\frac{\theta}{1-\theta}) + \ln(1 + w\theta) = 0 \tag{2.11}$$

Langmuir Isotherm

For $w = 0$, which is the interactionless case of adsorption, the Frumkin and Tempkin isothermes reduce to the Langmuir isotherm:

$$\Delta G_{ad} - q_e U + k_B T \ln(\frac{\theta}{1-\theta}) = 0 \tag{2.12}$$

2.4 Relevant Aspects of Electrochemistry

2.4.1 Redox Reactions

Oxidation

An atom is oxidised, when one or more electrons are removed:

$$\mathrm{X} \longrightarrow \mathrm{X}^+ + \mathrm{e}^- \tag{2.13}$$

In a more chemical way:

$$\mathrm{C} + \mathrm{O_2} \longrightarrow \mathrm{CO_2} \tag{2.14}$$

Here the electrons are "removed" from the carbon atom and "added" to the oxygen atoms in the sense that the chemical bond is polarized due to the more electronegative oxygen atom. Hence, the carbon atom is oxidized (The oxygen atoms are reduced in this reaction, as they gain electrons)

Reduction

This is the reverse reaction, which would be the addition of electrons:

$$\mathrm{X^+} + \mathrm{e^-} \longrightarrow \mathrm{X} \tag{2.15}$$

Or:

$$\mathrm{CO_2} \longrightarrow \mathrm{C} + \mathrm{O_2} \tag{2.16}$$

2.4.2 Cathode and Anodes

Akin to Murphy's law is the fact that there is a lot of confusion about the definition of anodes and cathodes. Now, in electrochemistry and specifically when it comes to electrolysis the definition is clear:

At the cathode, a reduction reaction takes place. Electrically, the cathode is the (more) negative terminal of the cell.

At the anode, an oxidation reaction occurs takes place and the anode is the (more) positive terminal of the cell.

For a galvanic cell (battery), the assignment of the chemical red/ox reactions is the same but the electrical polarity is reversed.

2.4.3 Anodic Dissolution of Copper

At a certain potential, the copper atoms from the surface of the electrode start to dissolve in the electrolyte:

$$\mathrm{Cu} \longrightarrow \mathrm{Cu^{2+}_{(aq)}} + 2\,\mathrm{e^-} \tag{2.17}$$

In our experiments, the dissolution of copper takes place at more cathodic potentials than the production of oxygen. Therefore the electrochemical window is effectively diminished for our purposes, because the dissolution reaction occurs inside the electrochemical window of water. As a result, the voltage range used in our experiments is limited by the HER in the cathodic direction and by the Cu dissolution in the anodic voltage direction.

2.4.4 Butler-Volmer equation

The Butler-Volmer model of electrode kinetics is described in detail in ref.[1] chapter 3 section 3. This equation describes the current produced by a simple redox electrode reaction (the copper dissolution or the hydrogen evolution reaction) which is potential dependent and concentration dependent:

$$j = j_0 \left\{ \frac{c_\mathrm{o}(0,t)}{c_\mathrm{o}^*} \exp\left[\frac{\alpha_\mathrm{a} z q_e}{k_B T}(U - U_r)\right] - \frac{c_\mathrm{r}(0,t)}{c_\mathrm{r}^*} \exp\left[-\frac{\alpha_\mathrm{c} z q_e}{k_B T}(U - U_r)\right] \right\} \tag{2.18}$$

Where, j is the total current, j_0 is the current at $U = U_r$ for each of the two reactions at constant concentrations, $c_\mathrm{o}(0,t)$ and $c_\mathrm{r}(0,t)$ are the time-dependent surface concentrations of the oxidized and reduced species, c_o^* and c_o^* are the constant bulk concentrations, α_a and α_c are the anodic and cathodic charge transfer coefficients, z the number of electrons involved, q_e is the elementary charge, U is the applied potential and U_r is the equilibrium potential, where there is no net current (ideal case, stirred solution). When we neglect the concentration dependence and look at medium overpotentials $(E - E_r)$, then the current is mostly exponential.

2.4.5 Reactions at the Cu(110) surface

In ref.[3], the following surface reactions are described:

$$\mathrm{Cl^-_{(aq)}} \rightleftharpoons \mathrm{Cl_{(ad)}} \tag{2.19}$$

$$\mathrm{Cu_{(bulk)}} + \mathrm{Cl_{(ad)}} + \mathrm{Cl^-_{(aq)}} \rightleftharpoons \mathrm{[CuCl_2]^-_{(aq)}} \tag{2.20}$$

$$\mathrm{Cu_{(bulk)}} + \mathrm{Cl_{(ad)}} \rightleftharpoons \mathrm{CuCl_{(s)}} \tag{2.21}$$

A Cl ion can adsorb from the solution (and return to the solution) at the surface. At potentials where Cl ions are adsorbed at the surface, $\mathrm{[CuCl_2]^-_{(aq)}}$ (solvated ion) or $\mathrm{CuCl_{(s)}}$ (surface precipitates) can be formed.

2.4.6 Diffusion

In resting solutions, the reactants have to diffuse from the bulk of electrolyte solution to the surface of the electrodes to partake in electrode reactions. The products then diffuse back to the solution. All of this is driven concentration gradients:

$$J_D = -D\frac{\partial c}{\partial x} \tag{2.22}$$

The diffusion flux is J_D and D is the diffusion coefficient and $c(x,t)$ is the concentration of a particular solute at a specified time.

With mass conservation this leads to:

$$\frac{\partial c}{\partial t} + \frac{\partial J_D}{\partial x} = 0 \tag{2.23}$$

$$\frac{\partial c}{\partial t} = D\frac{\partial^2 c}{\partial x^2} \tag{2.24}$$

Diffusion Limited Electrode Reactions

When a reaction at the electrode surface is limited in its speed by the rate that the reactants diffuse to the surface, then this reaction is called diffusion limited. In our context this is for example the copper dissolution. The Cl adsorption on Cu (110) is slightly diffusion limited, which is not the case at the Cu (111) surface.

In a CV scan, the peak current of a simple redox reaction would show this behaviour (ref.[5]):

$$i_p = 0.4463\, n q_e N_A A\, c\sqrt{\frac{n q_e s_r D}{k_B T}} \tag{2.25}$$

The Randles–Ševčík equation above describes the peak current i_p of a simple redox reaction like the HER or the Cu_2^+ dissolution. The peak current rises only with the square root of the scan rate, because the reactants need time to diffuse from the solution to the surface.

This diffusion limitation leads to the peaks having "tails" in the direction of the scan. Those can be described by a semiintegral of the "unlimited" peaks ref.[7] (chapter 11.2 about diffusion on electrode surfaces). The semiintegral acts like an integral with some kind of decaying "memory" in the sense that the value of the semiintegral in the time domain at a certain point is mostly determined by rather recent "peaks".

Semiintegral

The semiintegral ref.[7] (chapter 7 about semiderivatives and semiintegrals) can be defined in a hand-waving manner like this: if it is applied twice to a function, it gives a regular integral. One of the most convenient and straightforward ways (which omits several subtleties of non-integer order integration and is therefore not used in the book mentioned above) to define a semi-integral is in the Fourier domain:

$$\mathcal{I}_t^{1/2} f(t) = (\mathcal{F}^{-1} \sqrt{\frac{i}{\omega}} (\mathcal{F} f)(t))(\omega) \tag{2.26}$$

In the experiments, only the onset of the copper dissolution "peak" is visible. This onset is in good approximation exponential and would be exactly the same, but with reversed polarity, when the electrolyte would be stirred like the function $f(t)$ (see Fig. 2.4) below:

$$f(t) = e^t \Theta(-t) - e^{-t} \Theta(t) \tag{2.27}$$

where Θ is the Heaviside step function.

$$\mathcal{I}_t^{1/2} f(t) = e^t \, \Theta(-t) + (e^t (1 - \operatorname{erf}(\sqrt{t})) - \frac{e^{-t} \operatorname{erf}(i\sqrt{t})}{i}) \, \Theta(t) \tag{2.28}$$

here $\mathcal{I}_t^{1/2}$ is the semi-integral operator. For the sake of completeness the semi-integral of a gaussian is given below.

$$\mathcal{I}_t^{1/2} e^{\frac{-t^2}{2}} = \frac{\sqrt{\pi} e^{-\frac{t^2}{4}} \left(|t| I_{-\frac{1}{4}} \left(\frac{t^2}{4} \right) + t \, I_{\frac{1}{4}} \left(\frac{t^2}{4} \right) \right)}{2\sqrt{|t|}} \tag{2.29}$$

Above, $I_{-\frac{1}{4}}$ and $I_{\frac{1}{4}}$ are modified Bessel functions of the first kind.

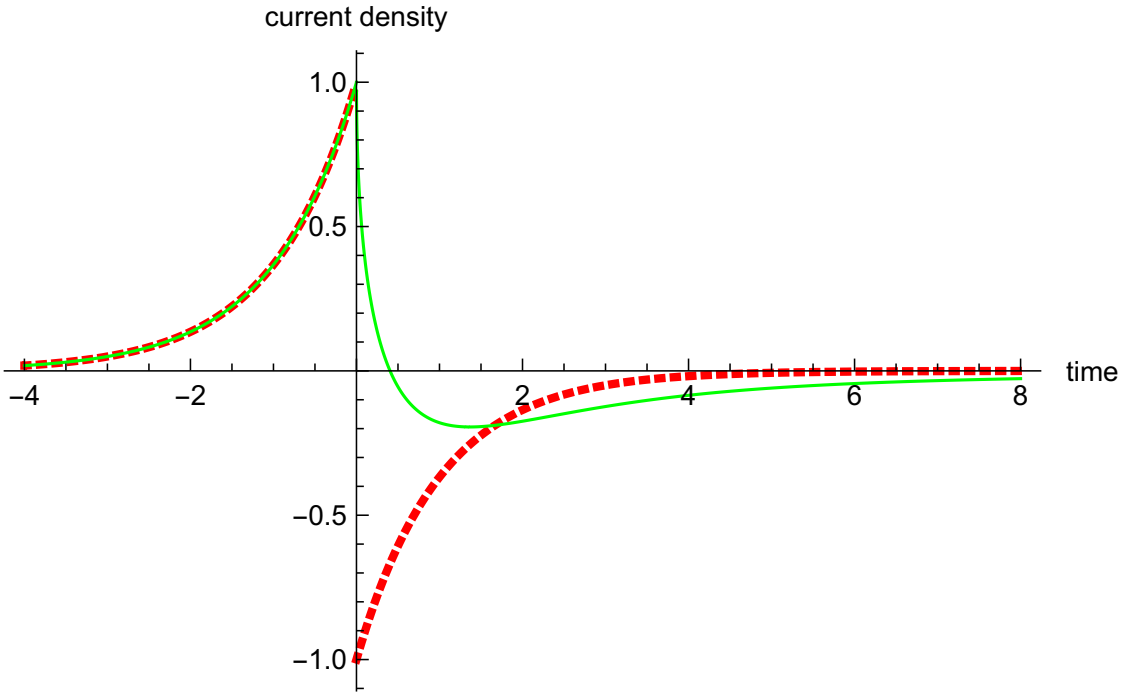

Figure 2.4: Exponential function(s) in red with discontinuity and the semi-integral of the red line in green, which is continuous (quite interesting) and very similar in shape to the Cu dissolution region in the CV scans as well as the hydrogen evolution region on the other side

2.5 Cyclic Voltammetry

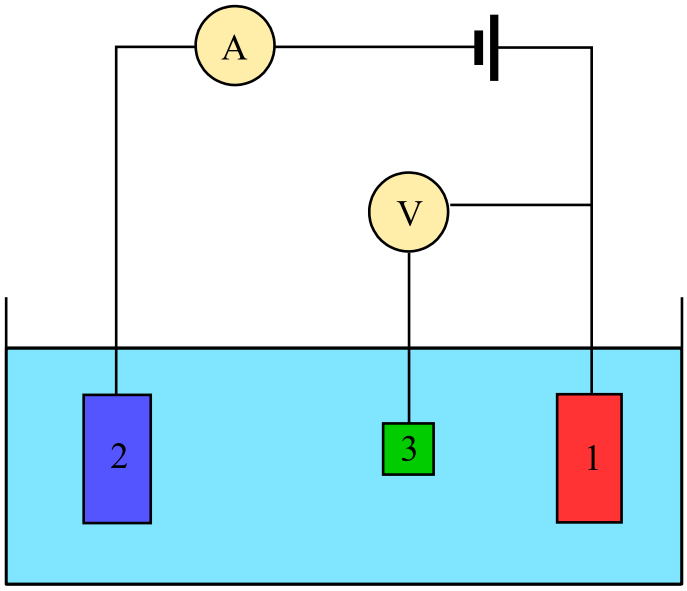

Figure 2.5: Principle of a typical CV setup[13]

Cyclic voltammetry is a commonly used method to gain insight into electrochemical electrode reactions. There are 3 electrodes used, which are all in contact with an electrolyte solution, which is not stirred or moved in any significant way. The first (1), the working electrode is the sample, which is under study. The second (2) electrode is the counter electrode which is there to close the electrical

circuit. The third electrode is the reference electrode (3). The reference electrode is very close to the surface of the working electrode and it is connected to a potentiostat with a large electrical resistance. If there is a current flowing between (1) and (2), then there is a voltage drop in the electrolyte, which is due to the electrical resistance of the electrolyte. The purpose of the reference electrode is to measure solely the voltage drop that occurs at the surface of the working electrode. To avoid measuring this so-called ohmic voltage drop, the reference electrode has to be as close as possible to the surface of the working electrode. Now the potentiostat applies a voltage between the working electrode and the counter electrode, such that the desired time dependent voltage between the reference electrode and the working electrode is reached and maintained.

In cyclic voltammetry, linear voltage sweeps (see Fig. 2.6) are applied cyclically between reference electrode and the working electrode in a zig-zag way while the current is measured:

$$\mathrm{U}(t) = \begin{cases} U_1 + s_r \cdot (t \bmod p), & \text{if} \quad t \bmod p < \frac{p}{2} \\ U_2 - s_r \cdot (t \bmod \frac{p}{2}), & \text{otherwise} \end{cases} \tag{2.30}$$

The lowest voltage is U_1 and the highest voltage is U_2. The period p of one cycle is determined by the constant scanrate s_r. With $t \bmod p$ the modulo operation (which is the remainder of $t : p$) is denoted. This leaves us with:

$$p = 2\frac{U_2 - U_1}{s_r} \tag{2.31}$$

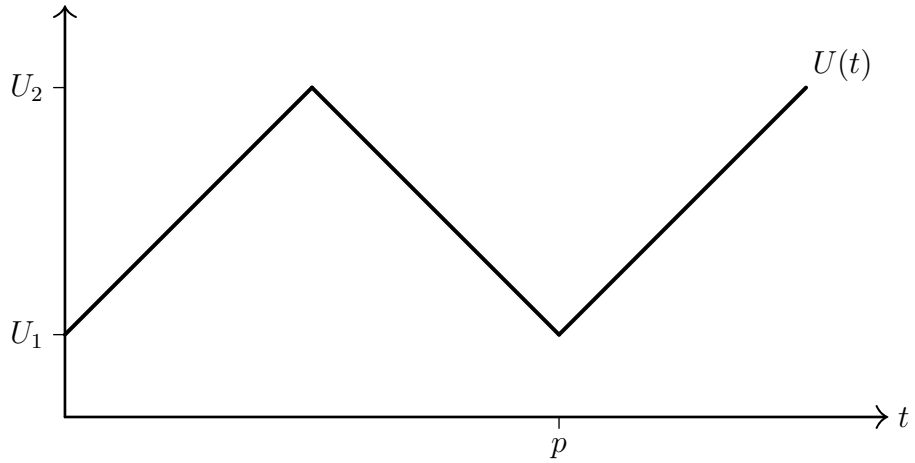

Figure 2.6: Linear voltage scan which is used in cyclic voltammetry. The reversal points are U_1 and U_2.

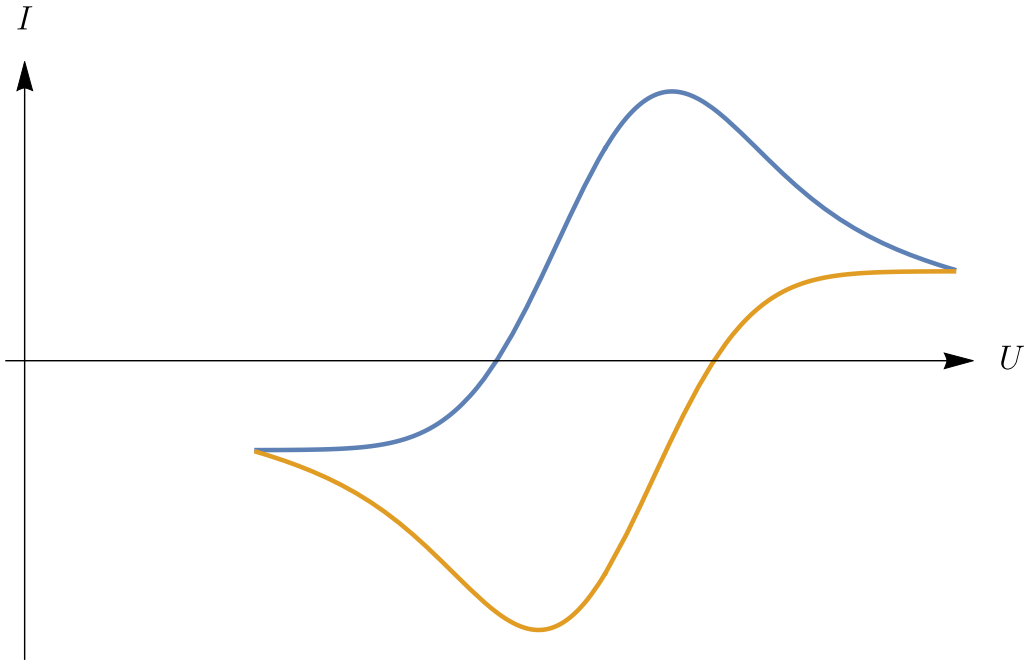

Figure 2.7: Well behaved cyclic voltammogram for a simple redox reaction like the copper dissolution, with no Cl adsorption and desorption peaks and no electronic charging currents (change in surface electron excess) shown. The peaks for the Cu dissolution and redeposition both are shifted from their equilibrium position, because the redox reaction is diffusion limited (see section about diffusion and subsection about semiintegral above), as the electrolyte is not in motion like in hydrodynamic voltammetry. However, in the experiments for this thesis only the onset of the peaks show up in the CV scans, because the main interest is adsorption of Cl and not Cu dissolution. Therefore the scan range is restricted, which prevents excessive sample damage.

Now, much of the electrochemistry of adsorption at the working electrode can be modeled by a capacitor:

$$C = \frac{dQ}{dU} \tag{2.32}$$

$$Q = \int_0^U C(U')dU' \tag{2.33}$$

$$I = \frac{dQ(U)}{dt} = \frac{dQ(U)}{dU}\frac{dU(t)}{dt} \tag{2.34}$$

Which gives for $U(t) = U_1 + s_r t$:

$$I = C(U(t))\frac{dU(t)}{dt} = C(U_1 + s_r t)s_r \tag{2.35}$$

So, a capacitor with voltage dependent capacitance $C(U)$ would show the profile of the effective capacitance in the current flowing trough it. This would still be true if $C(U)$ would be shifted due to diffusion effects when changing the scanrate, as long as the scranrate is constant for every cycle. This is the reason why cyclic voltammetry enables the study of adsorption processes. This effective capacitance can be divided into two parts: adsorption of ions (ref.[19]) and charging of the interface due to changing voltage, which changes the surface electron excess:

$$I[U(t)] = C\frac{dU}{dt}\bigg|_{\theta} + n\Gamma_{I,\max}A\frac{\delta\theta}{\delta U}\frac{dU}{dt}\bigg|_{\Gamma_{\text{free}}} \tag{2.36}$$

The first term represents the charging of the interface due to a change in the applied voltage (at contant surface coverage θ). This means, that the surface electron excess Γ_e and the number of ions in the diffuse double layer Γ_{free} change. This contribution is rather small.

The second term denotes the adsorption/desorption of ions, while the number of ions in the diffuse layer is held constant. This current contribution is proportional to the change in surface coverage and the total electrode area A. The maximum number of ions that can be adsorbed per unit area is $\Gamma_{I,\max}$.

In general, C depends on the applied potential and the change in the surface coverage can depend on the speed at the ions diffuse to the surface (diffusion limitation).

3 Second Harmonics Generation

3.1 Nonlinear Optics Basics

Nonlinear optics is a branch of optics, that exploits the nonlinear effects, that occur in many media, with coherent light at very high intensities. The invention of the laser in the 1960s kickstarted the research in the field due to the now possible high intensities of focused laser light.

The electric displacement field $\mathbf{D}$ describes an external electrical field $\mathbf{E}$ and the response of matter to it:

$$\mathbf{D} = \varepsilon_0 \mathbf{E} + \mathbf{P} \tag{3.1}$$

Matter responds to an electrical field by creating dipoles or moving existing ones. This is expressed by the polarization density $\mathbf{P}$ and ε_0 is the vacuum permittivity.

For low light intensity (no lasers), $\mathbf{P}$ can be expressed as follows:

$$\mathbf{P} = \varepsilon_0 \chi \mathbf{E} \tag{3.2}$$

The polarisation density increases proportional to the electric field. The constant χ is called electric susceptibility. For now, we only consider isotropic media for the sake of simplicity. But what happens, when the electric field is strong enough for this (very good) approximation to break down? Well, we do what works very often: Taylor expansions!

$$\mathbf{P} = \varepsilon_0 \sum_n \chi^{(n)} \mathbf{E}^n = \varepsilon_0 \left(\chi^{(1)} \mathbf{E} + \chi^{(2)} \mathbf{E}^2 + \chi^{(3)} \mathbf{E}^3 + \dots \right) \tag{3.3}$$

Here, we made a simple Taylor expansion of $\mathbf{P}$ in powers of $\mathbf{E}$ and $\chi^{(1)}$ is the normal linear electric susceptibility, where $\chi^{(2)}$, $\chi^{(3)}$ are the higher order nonlinear contributions, which are several orders of magnitude smaller than $\chi^{(1)}$.

For metals, calculations are often carried out using the polarisation current density $\mathbf{j}_p$, which is related to the polarisation $\mathbf{P}$:

$$\mathbf{j}_P = \frac{\partial \mathbf{P}}{\partial t} \tag{3.4}$$

It is important to note, that the polarisation density itself does not propagate (at least in dielectrics). But it radiates:

$$\mathbf{H} = \frac{ck^2}{4\pi} (\hat{\mathbf{n}} \times \mathbf{p}) \frac{e^{ikr}}{r} \tag{3.5}$$

$$\mathbf{E} = Z_0 \mathbf{H} \times \hat{\mathbf{n}} \tag{3.6}$$

$$= Z_0 \frac{ck^2}{4\pi} (\hat{\mathbf{n}} \times \mathbf{p}) \frac{e^{ikr}}{r} \times \hat{\mathbf{n}} \tag{3.7}$$

$$= Z_0 \frac{ck^2}{4\pi} \frac{e^{ikr}}{r} (\mathbf{p} - (\mathbf{p} \cdot \hat{\mathbf{n}}) \hat{\mathbf{n}}) \tag{3.8}$$

$$= Z_0 \frac{ck^2}{4\pi} \frac{e^{ikr}}{r} (\bar{E}_3 - \hat{\mathbf{n}}\hat{\mathbf{n}}) \mathbf{p} \tag{3.9}$$

Above, $\mathbf{H}, c, k, \hat{\mathbf{n}}, \mathbf{p}, r, \bar{E}_3$ and Z_0 are the magnetic field strength, speed of light, length of the wave vector, normal unit vector in direction of observation, dipole moment of considered entity, radius, unity matrix, and the free space impedance. We start with (9.20) in ref[6] which describes the far field dipole radiation ($\propto \frac{1}{r}$) and then we use the triple product expansion for the vector triple product. This is for one dipole but it is equally valid for a polarisation density.

3.2 Second Harmonics Generation

Let's assume we have a suitable medium, where only $\chi^{(2)}$ is not zero. (I should mention here that this can't be a medium with inversion symmetry in its crystal structure, given certain assumptions)

Now, we have a coherent type of electromagnetic radiation: a plane wave:

$$E(t) = E_0 \sin \omega_0 t \tag{3.10}$$

If we insert this into (3.3) and take only the second order term, we get:

$$|\mathbf{P}^{(2)}| = \varepsilon_0 \chi^{(2)} E^2 = \varepsilon_0 E_0^2 \chi^{(2)} \sin^2 \omega_0 t \tag{3.11}$$

Remembering $\sin^2(x) = \frac{1-\cos(2x)}{2}$ we arrive at:

$$|\mathbf{P}^{(2)}| = \frac{1}{2}\left(\varepsilon_0 E_0^2 \chi^{(2)} - \varepsilon_0 E_0^2 \chi^{(2)} \cos 2\omega_0 t\right) \tag{3.12}$$

The first term is an effect called optical rectification, because the resulting polarization density is not time dependent. The second term represents a polarization density, that oscillates at twice the frequency of the exciting field, hence this effect is called second harmonic generation (SHG).

For this process to be efficient for beams propagating in bulk materials, the fundamental and the second harmonic wave have to have the same, fixed phase relationship throughout the whole crystal:

$$n(\omega_0) = n(2\omega_0) \tag{3.13}$$

Now, this can't be the case in materials with isotropic properties, as the dispersion of the refractive index prevents the condition given above from being fulfilled. So people use most of the time materials like BBO (β-Barium borate).

Those materials feature anisotropy in their refractive index. In BBO there are 2 crystal directions with $n = n_o = 1.6776$ (ordinary refractive index) and one direction with $n = n_e = 1.5534$ (extraordinary refractive index).

If the electric field points in one of these main directions, the corresponding electromagnetic wave experiences n_o or n_e. By adjusting the crystal orientation and/or the beam polarisation the condition above can be fulfilled. It also helps that in BBO n_o and n_e have a similar and rather flat dispersion.

When SHG appears not in bulk materials but at external surface reflections, the efficiency is generally quite low, as there is no phase matching in the above sense possible and the interaction volume is very small.

3.3 SHG, Symmetry and Surfaces

I want to mention for clarity that the derivations above assume, that the dipole approximation holds, which may not always be the case. This means that for the description of the polarisation density we assume it to be always a density of dipoles, as the size of the bonds and atoms is always much smaller than than the wavelengths of visible light, so that the dipole term fiercely dominates.

When an electron oscillates around its resting position in a molecular bond / electron gas, there is an oscillating dipole moment present. In (very good) first order approximation the electron in its potential is like a harmonic oscillator (see Fig. 3.1). But at high electric fields the potential becomes more and more nonlinear. Then, there are two important cases: the potential can be centrosymmetric relative to the position with lowest energy or not. If the potential is centrosymmetric, then the lowest nonlinear component of the generated radiation is cubic in powers of the electric field. When we think of a fourier expansion of the oscillation of the dipole (see fig. 3.1), then the lowest nonlinear component has to have the same direction as the driving electric field, when the dipole is at the reversal points on both sides and the potential is smaller than a harmonic one at large amplitudes. In this way the amplitude of the oscillation is exaggerated (hyperpolarisation), as the electron can move farther out because the potential is flatter there.

Only the third harmonic can do this. So, in materials, which have their electrons in centrosymmetric potentials, SHG cannot occur in the bulk of the material, when the gradient of the electric field is negligible. An example would be silicon or an amorphous material like glass. But, when the potentials are asymmetric, SHG can occur in the bulk. One example would be GaN as the two different kinds of atoms gallium and nitrogen introduce some asymmetry in the bonds.

Copper has inversion symmetry (fcc lattice), so SHG would be forbidden in the bulk, but the electric field gradient at the surface is not negligible, because incoming light is mostly reflected and therefore attenuated exponentially over several hundred Å starting from the surface.

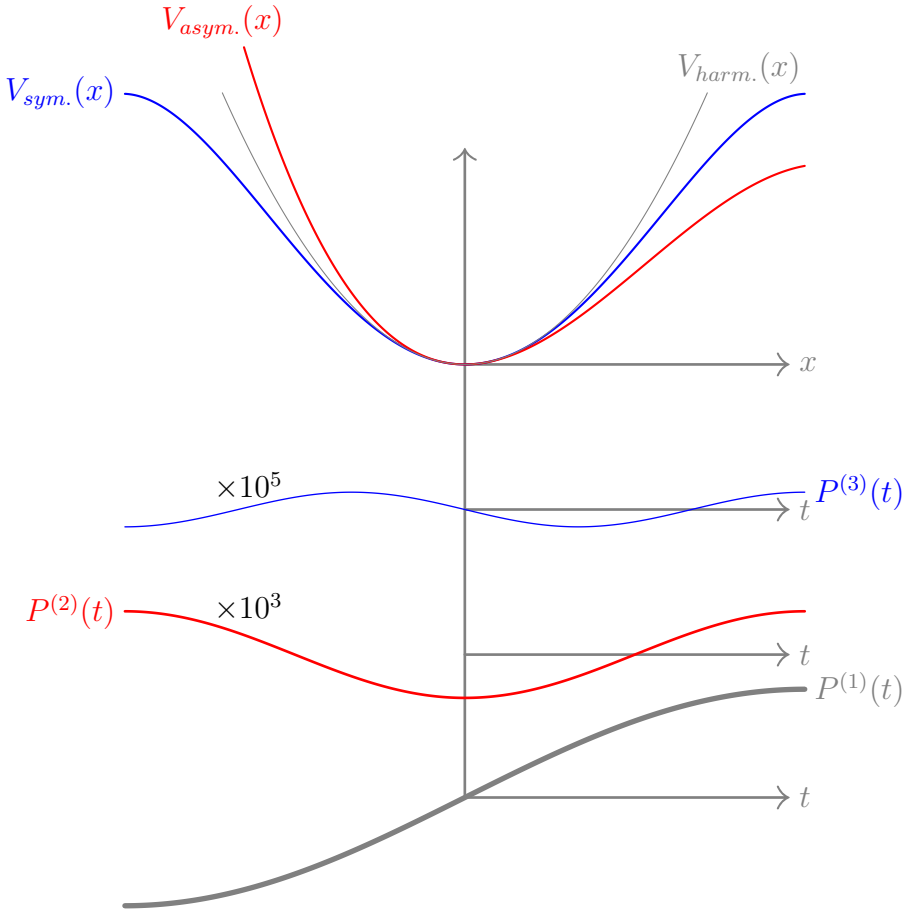

Figure 3.1: Electron in a symmetric potential with depictions of higher order polarizations

3.3.1 Surface and Symmetry Breaking and the Dipole Approximation

The following remarks in this (sub-)section are largely inspired by ref.[4]. At surfaces like in Fig. 3.2, the translational symmetry of the crystal is severely broken in the direction of the surface normal, because the crystal just ends! This often leads to a relaxation or even reconstruction of the surface. So the atoms at the surface may shift their positions or rearrange or both happens, because half of their binding partners are not existing. Due to this fundamental asymmetry at the surface (no inversion symmetry at all in the direction of the surface normal), it is possible to generate SHG photons at surface reflections or more generally, at interfaces.

The reason for this is twofold: The first one is that electrons can move more easily in the direction of the bulk than out of the material (anharmonicity and asymmetry). This leads to the electric dipole contribution at the surface to the SHG response.

Moreover, in the direction of the surface normal, the normal component of the electric field changes in a very short distance. This means that in this direction the electric dipole approximation, which states the opposite, namely that on the scale of atoms, the electric field is basically constant is not valid. Because of that, the electric quadrupole contribution comes into play.

I did some perturbation calculations with a harmonic oscillator with a linearly varying electric field (in space) and this already shows 2nd order effects with no anharmonicity terms in the oscillator potential. Intuitively this is clear: when we are, for example well below the resonance frequency of the HO and pull harder on one side than on the other, then the displacement will be larger on this side, which means we have a second order component in the displacement, when the driving force varies harmonically in time. This means that the dipole approximation is not true any more, which means that there is a quadrupolar contribution to the SH response. This is important because at the surface of every metal there is a strong, localized electric field (surface dipole). This electric field is localized in a region that is much smaller than the wavelength of the incident radiation and therefore the dipole approximation is not valid in the direction of the surface normal.

3.4 High Level Considerations of Surface SHG

Before we dive in to some models of surface SHG, I want to give an overview about the different possible contributions to the SH response of an interface. From a general, macroscopic point of view, there are several contributions that can add to the overall SHG response of an interface between two materials:

interface:	el. dipole	el. quadrupole.	mag. dipole	EFISHG
bulk:	~~el. dipole~~	el. quadrupole	mag. dipole	~~EFISHG~~

Table 3.1: Overview of possible contributions from the bulk and the interface of 2 materials with inversion symmetry, the forbidden and "quasi-forbidden" are crossed out

If both media posses a crystal structure, which has a center of inversion or if they are amorphous, then the *electric dipole* contribution, which is the strongest of all the contributions is forbidden in the bulk of the materials and allowed only at the interface (see Table 3.1) due to the breaking of the inversion symmetry as explained above. In 3.7, a surface dipole contribution is calculated on basis of the SBHM. Further, some symmetry arguments are presented in 3.5, which apply to the electric dipole contribution.

Then there is the *electric quadrupole* contribution, which arises from a nonvanishing gradient in the electric field. In the bulk of the copper, this is due to an exponential decline of the electric field

strength into the metal due to the shielding currents. At the surface, the normal component of the electric field varies even faster on the order of Å, which causes an electric quadrupole contribution. Some quadrupole contributions are calculated in 3.6.3.

The *magnetic dipole* contribution is often neglected in insulators, but seems to be important in metals like silver and gold (see ref.[2]). There, the contribution arises from the Lorentz force that acts on the free electrons.

And finally, there is *EFISHG* (electric field induced second harmonics generation), which is a third order effect and is enabled by extremely large electric DC fields ($\approx 10^9$ V), which appear in our copper-electrolyte system only at the surface due to the Helmholtz double layer, which acts as a capacitor with an extremely small plate separation and therefore a strong internal electric field. In addition, due to the diffuse layer, this strong electric field extends some Debye-lengths in to the electrolyte.

To sum it up, the suppression of the bulk dipole contribution enables (in principle) a high surface sensitivity of surface SHG measurements.

3.5 Symmetry Considerations of the ideal Cu (110) Surface

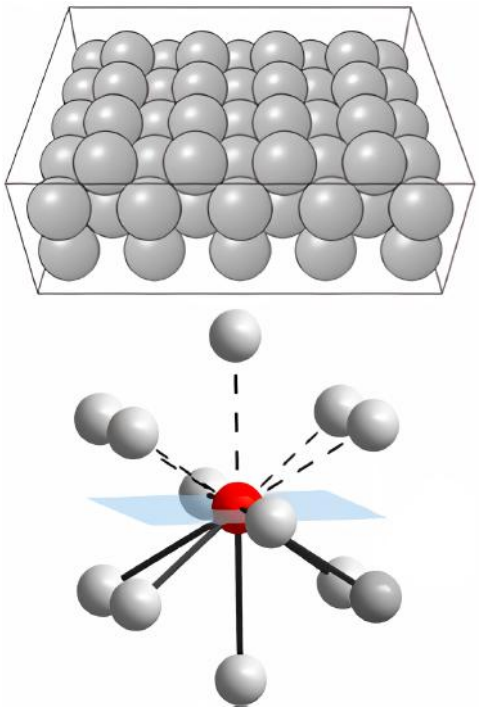

Figure 3.2: fcc (110) surface with nearest neighbours shown below[8]. The rows at he surface are aligned with the $[1\bar{1}0]$ direction, while the direction normal to the rows is the [001] direction.

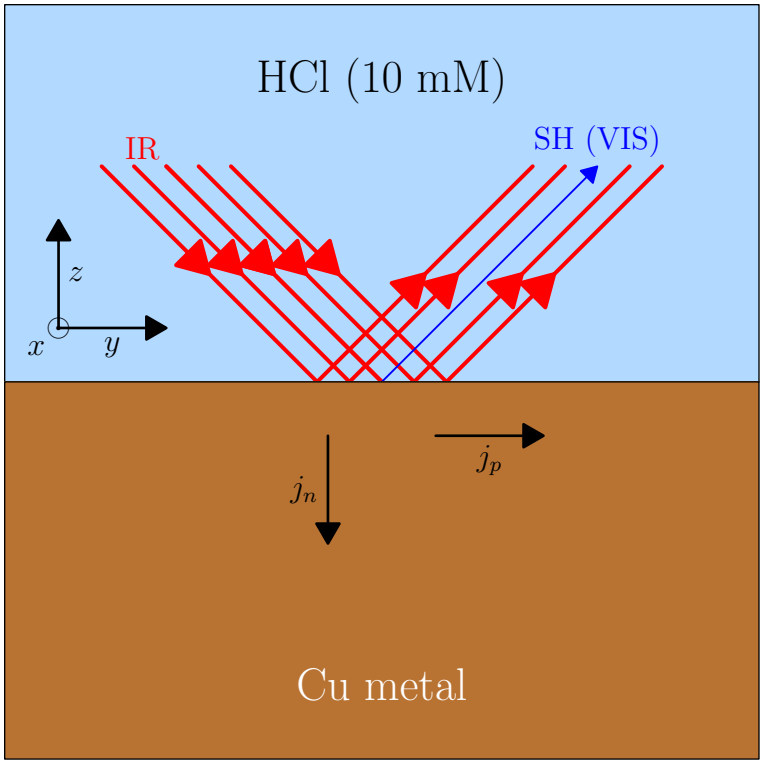

Figure 3.3: Diagram of the rays involved with coordinate axes (x-axis points towards the reader)

On copper (111), the adsorption sites of the Cl ions are known, while on copper (110) this is not the case, because the adsorption process triggers some additional surface reactions/transformations[17]. It may also be that the Cl ions are too mobile on the surface for good EC-STM images.

Below, some symmetry considerations of the ideal copper (110) surface are presented, to get a basic idea (in el. dipole approximation) of what to expect from measurements.

The basic notions of crystal symmetry and their representations with tensors are taken from ref.[11]. The 2D surface of copper (110) exhibits rectangular symmetry, as the topmost copper atoms form rows. Now, one can argue, that the point group of the surface belongs to the symmetry group C_{2v}. The surface can be rotated 180° around the surface normal and it stays the same. And there are two mirror planes perpendicular to the surface normal and aligned along the rows of the topmost copper atoms and perpendicular to those rows. The most general form of a third order tensor, which is used to describe some of the (anisotropic) properties of a material is shown below and this tensor has 27 coefficients:

$$d_{ijk} = \left(\begin{pmatrix} d_{1,1,1} & d_{1,1,2} & d_{1,1,3} \\ d_{1,2,1} & d_{1,2,2} & d_{1,2,3} \\ d_{1,3,1} & d_{1,3,2} & d_{1,3,3} \end{pmatrix} \begin{pmatrix} d_{2,1,1} & d_{2,1,2} & d_{2,1,3} \\ d_{2,2,1} & d_{2,2,2} & d_{2,2,3} \\ d_{2,3,1} & d_{2,3,2} & d_{2,3,3} \end{pmatrix} \begin{pmatrix} d_{3,1,1} & d_{3,1,2} & d_{3,1,3} \\ d_{3,2,1} & d_{3,2,2} & d_{3,2,3} \\ d_{3,3,1} & d_{3,3,2} & d_{3,3,3} \end{pmatrix} \right) \tag{3.14}$$

But the C_{2v} symmetry of the Cu(110) surface imposes constraints on the associated matter tensors. The tensor has to be invariant under the symmetry operations which form the C_{2v} symmetry group. Now, a lot of the tensor components are zero:

$$^{C_{2v}}d_{ijk} = \left(\begin{pmatrix} 0 & 0 & d_{1,1,3} \\ 0 & 0 & 0 \\ d_{1,3,1} & 0 & 0 \end{pmatrix} \begin{pmatrix} 0 & 0 & 0 \\ 0 & 0 & d_{2,2,3} \\ 0 & d_{2,3,2} & 0 \end{pmatrix} \begin{pmatrix} d_{3,1,1} & 0 & 0 \\ 0 & d_{3,2,2} & 0 \\ 0 & 0 & d_{3,3,3} \end{pmatrix} \right) \tag{3.15}$$

So, only 7 nonzero tensor components remain and those can be described by 5 independent parameters as we will see later.

Now, we name this tensor second order electric susceptibility and apply some electric fields to it to get some second order polarisation going:

$$\mathbf{P_2} = \chi_2 \cdot \mathbf{E} \cdot \mathbf{E} \qquad \mathbf{E} = \{E_x, E_y, E_z\} \tag{3.16}$$

The coordinate system is shown in Fig. 3.3.

$$\mathbf{P_2} = \begin{pmatrix} (\chi_{1,1,3} + \chi_{1,3,1})\, E_x E_z \\ (\chi_{2,2,3} + \chi_{2,3,2})\, E_y E_z \\ \chi_{3,1,1} E_x^2 + \chi_{3,2,2} E_y^2 + \chi_{3,3,3} E_z^2 \end{pmatrix} \tag{3.17}$$

For s- and p-polarized input pulses (where $E = E_x$ and $E_x = 0$ respectively), the second order polarisation is then:

$$\mathbf{P_{2,s}} = \begin{pmatrix} 0 \\ 0 \\ E_x^2 \chi_{3,1,1} \end{pmatrix} \tag{3.18}$$

and:

$$\mathbf{P_{2,p}} = \begin{pmatrix} 0 \\ E_y E_z \left(\chi_{2,2,3} + \chi_{2,3,2}\right) \\ \chi_{3,2,2} E_y^2 + E_z^2 \chi_{3,3,3} \end{pmatrix} \tag{3.19}$$

Now, the far field radiation (see equ. 3.9) can be calculated:

$$\mathbf{E}_f \propto (\bar{E}_3 - \hat{\mathbf{n}}\hat{\mathbf{n}})\mathbf{P_2} \tag{3.20}$$

This is a projection of the polarisation vector into the normal plane of the k-vector of the reflected beam (45° exit angle).

For s- and p-polarized input pulses (where $E = E_x$ and $E_x = 0$ respectively (see. Fig. 3.3 for coord. system)), the second order far field radiation is then:

$$\mathbf{E}_{f,s} \propto \begin{pmatrix} 0 \\ \frac{1}{2} E_x^2 \chi_{3,1,1} \\ \frac{1}{2} E_x^2 \chi_{3,1,1} \end{pmatrix} \tag{3.21}$$

$$\mathbf{E}_{f,p} \propto \begin{pmatrix} 0 \\ \frac{1}{2}\left(\chi_{3,2,2} E_y^2 + E_z \left(\chi_{2,2,3} + \chi_{2,3,2}\right) E_y + E_z^2 \chi_{3,3,3}\right) \\ \frac{1}{2}\left(\chi_{3,2,2} E_y^2 + E_z \left(\chi_{2,2,3} + \chi_{2,3,2}\right) E_y + E_z^2 \chi_{3,3,3}\right) \end{pmatrix} \tag{3.22}$$

now we can simulate the effect of the analyser prism in s-position and therefore block the E_y and E_z component:

$$\mathbf{E}_{f,ss} \propto \begin{pmatrix} 0 \\ 0 \\ 0 \end{pmatrix} \tag{3.23}$$

Within this model, we should measure no SH radiation in ss-polarisation, which is interesting. In addition, we can simulate the effect of the analyser prism in p-position and therefore block the E_x component only, which is zero anyway:

$$\mathbf{E}_{f,pp} \propto \begin{pmatrix} 0 \\ \frac{1}{2}\left(\chi_{3,2,2} E_y^2 + E_z \left(\chi_{2,2,3} + \chi_{2,3,2}\right) E_y + E_z^2 \chi_{3,3,3}\right) \\ \frac{1}{2}\left(\chi_{3,2,2} E_y^2 + E_z \left(\chi_{2,2,3} + \chi_{2,3,2}\right) E_y + E_z^2 \chi_{3,3,3}\right) \end{pmatrix} \tag{3.24}$$

and let us calculate the intensity (setting $E_y = E_z = |\mathbf{E}|/\sqrt{2}$, since the incidence angle is 45°):

$$I_{pp} \propto \frac{1}{8} E^4 \left(\chi_{2,2,3} + \chi_{2,3,2} + \chi_{3,2,2} + \chi_{3,3,3}\right)^2 \tag{3.25}$$

which is proportional to the square of the sum of 4 tensor components.

A rotation around surface normal (when the sample is not probed along the [110] or [1$\bar{1}$0] direction) just rotates the direction of tensor components probed by I_{pp} in the xy-plane, while I_{ss} stays zero.

This derivation only considers symmetry properties and gives no (microscopic) explanation of the origin of SH radiation or the responsible mechanisms. The one interesting result is that, if some SH intensity could be detected in *ss*-polarisation, then this could indicate "symmetry breaking" (int the dipole approximation), in the sense that there are morphological features at the surface, that deviate from the C_{2v} symmetry of the Cu (110) surface. In reality, there might be a quadrupole term that is quite weak or the sample is unintentionally tilted by a slight amount.

The presence of the electrolyte (mostly water) does not alter the symmetry properties of the surface as it is homogeneous and isotropic, when we assume statistical orientations (not always true). On average, the copper surface will even "impose" its symmetry properties onto the watery side of the interface.

3.6 SHG in Metals

While SHG in single crystalline semiconductors, can be described often by a simple anharmonic oscillator model, where the electrons oscillate in straight lines along the bonds, this approach does not work in metals, but it may work for surface adsorbates. The free and the not-so free electrons behave quite linear as it is quite hard to elicit a nonlinear response.

3.6.1 Mechanisms for SHG in Cubic Metals

The following calculations and ideas (from here to equ. 3.37) regarding the free electron gas are mainly taken from[16]. Because the second order response is quite small, a pertubative treatment is appropriate. So at the beginning, the first order electric fields are determined and then those are used to calculate the second order current densities. Those are in turn used to calculate the second order far field radiation.

Cubic metals have a crystal structure that is inversion symmetric, which should result in no SHG response for constant electric fields. However, if there is a gradient in the electric field, things are different, as contributions do not cancel out perfectly any more. Also, the current density becomes a non-local quantity as it depends on the electric field in a region and not only at a single point. This occurs especially at the surface, where the surface dipole creates a strong localized electric field and the linear electric fields coming from the outside have a gradient due to exponential decay in the material.

A second, related mechanism, which is not quite the same is the breaking of inversion symmetry at the surface. The existence of the surface restricts the motion of electrons in one (outward) direction and creates an asymmetry which gives rise to SH currents.

3.6.2 Types of SH Currents

In general, there are 3 types of SH currents, that can contribute to the surface SH response of a metal[10]:

- There a current in the bulk of the metal, which extends several hundred Å below the surface in a region, whose extent is the skin depth λ_{skin}. This current is parallel to the electric field

and therefore does not radiate in the direction of the reflected beam except near the surface. This type of current is mostly insensitive to surface conditions, which affect only a few of the topmost Å of the material.

- Normal surface current: This current is localized at the surface and normal to it. It depends heavily on the makeup of the surface in the normal direction as this determines the gradient of the electric field across the boundary. This current is the stronger one of the surface currents. This is due to the lack of inversion symmetry normal to the surface, which restricts the motion of the electrons.

- Parallel surface current: This current is localized at the surface and parallel to it. It is sensitive to surface scattering of the electrons, which for example, depends on surface morphology.

3.6.3 Model: Free Electrons in the Long Wavelength Limit

For a correct and complete treatment of the SHG response of metals quantum mechanical calculations are required. While for the parallel surface currents this is not necessary, the normal currents do not allow the long wavelength limit and the local field approximations, as the electric field varies too rapidly across the surface.

Such calculations, are beyond the scope of this thesis and therefore we restrict ourselves here to a model, which still give us some important insights.

Assumptions

Free electrons in the classical sense make up the metal. The boundary is smooth and has no roughness. The metal occupies the negative half-space in z-direction. We assume, that the local approximation holds, which states that the electric fields do not vary faster than the wavelength of the incident radiation. The equation below is derived from a hydrodynamic model[2] for the electrons. In this case the electron gas is treated as a classical fluid with constant pressure and zero viscosity (Navier-Stokes equations). The fluid then interacts with electromagnetic fields $(\mathbf{E}, \mathbf{H})$ and starts to flow and to vary its density n and velocity $\mathbf{v}$:

$$\frac{\partial \mathbf{v}}{\partial t} + (\mathbf{v} \cdot \nabla)\mathbf{v} = -\frac{q_e}{m^*}(\mathbf{E} + \frac{1}{c}\mathbf{v} \times \mathbf{H}) \tag{3.26}$$

$$\nabla \cdot \mathbf{E} = -4\pi q_e(n - n_0) \qquad \frac{\partial n}{\partial t} = -\nabla \cdot (n\mathbf{v}) \tag{3.27}$$

The two equations above are the first Maxwell equation and the continuity equation and $m^*, -q_e$ are the effective mass and the charge of an electron. This system of equations can be solved by perturbation theory in a self consistent manner for the second order current density (the influence of the magnetic field has been neglected):

$$\mathbf{j}_2(\mathbf{r}) = \frac{n_0 q_e^3}{i m^2 \omega^3}\left[\tfrac{1}{4}\nabla(\mathbf{E} \cdot \mathbf{E}) + \mathbf{E}(\nabla \cdot \mathbf{E})\right] \tag{3.28}$$

here, n_0 is the electron density, e_0 is the electron charge and m its mass. The expression above assumes, that the we already know the linear electric fields $\mathbf{E}$ in the material and at the surface.

Calculations

A quick look a the equation above says, that a field gradient is needed for second order currents to arise. Furthermore, the so-called convective acceleration $(\mathbf{v}\cdot\nabla)\mathbf{v}$ of the fluid (a fluid is accelerating, when it passes trough a converging nozzle), which is associated with the fluid dynamics equations is one source of nonlinearity [1] (and in general the reason, why real problems in fluid dynamics are hard to solve).

The first term contributes in the bulk and at the surface, while the second term only contributes at the surface. The second term is non-zero if there are net charges present, which is the case at the surface when we think of the surface dipole of a metal.

We take the second term of 3.28 and look only a the contribution parallel to the surface (for which the local approximation holds):

$$\mathbf{j}_{2\parallel}(\mathbf{r}) \propto \mathbf{E}_{\parallel}\frac{dE_z}{dz} \tag{3.29}$$

Above, $\mathbf{j}_{2\parallel}$ is the SH current component, which is parallel to the surface and $\mathbf{E}_{\parallel}$ is the parallel component of the (incident) electric field, while E_z is the normal component of the electric field.

Next, we consider the current from the classical hydrodynamical model, which treats the electron gas like a fluid to account for the electron-electron interaction:

$$\mathbf{j}_2 = n_0\mathbf{v}_2 + n_1\mathbf{v}_1 \tag{3.30}$$

Here, n_0 is the electron density without electromagnetic fields, n_1 is the change in electron density linear in the EM fields, v_1 is the velocity change of the electrons linear in the fields and v_2 is the second order velocity change.

Only the second term contributes to the parallel current (result from hydrodynamical calculations) therefore, the second order current depends only on the linear fields.

Now, we can obtain n_1 from this long-wavelength relationship with $\mathbf{P}_1$ as the linear polarisation:

$$n_1 = -\nabla\cdot\mathbf{P}_1 \tag{3.31}$$

And with some electrodynamics:

$$\mathbf{D}_1 = \mathbf{E}_1 + 4\pi\mathbf{P}_1 = \epsilon_1\mathbf{E}_1 \tag{3.32}$$

$$\mathbf{j}_1 = -n_0 q_e \mathbf{v}_1 \tag{3.33}$$

and the free electron gas:

$$\mathbf{v}_1 = \frac{-iq_e\mathbf{E}_{\parallel}}{m\omega} \tag{3.34}$$

when put together:

$$\mathbf{j}_{2\parallel} = \frac{iq_e\mathbf{E}_{\parallel}(\nabla\cdot\mathbf{P}_1)}{m\omega} \tag{3.35}$$

which can be rewritten with equation 3.31 as:

[1] In discussions with my supervisor Prof. Kurt Hingerl, we came to the conclusion that the convective acceleration is probably not the main source of nonlinearity, that causes SH effects. In hindsight, the continuity equation (see equ. 3.27, right equation) is more likely the source of the SH effects (see also 3.30). When the $(\mathbf{v}\cdot\nabla)\mathbf{v}$ is neglected, then equation becomes Drude-like with the mean free time between collisions with copper atoms $\tau\to\infty$.

$$\mathbf{j}_{2\parallel} = -\frac{iq_e\mathbf{E}_\parallel}{4\pi m\omega}\nabla\cdot\Big(\frac{4\pi n(\mathbf{r})q_e^2}{m\omega^2}\,\mathbf{E}(\mathbf{r})\Big) \tag{3.36}$$

when we remember the dielectric function of the ideal free electron gas:

$$\epsilon = 1 - \frac{\omega_p^2}{\omega^2} \qquad \omega_p^2 = \frac{4\pi n_e q_e^2}{m_e} \qquad \mathbf{P} = \frac{(\epsilon-1)}{4\pi}\mathbf{E} \tag{3.37}$$

If we assume that the electron density at the surface can be written as:

$$n(\mathbf{r}) = n_0(\mathbf{r}) + n_s(z, \sigma(U_{int})) \tag{3.38}$$

which just means we have a constant (when the voltage U_{int} changes) part $n_0(\mathbf{r})$ and a part $n_s(z, \sigma(U_{int}))$ that varies with the applied voltage U_{int} across the interface. The surface charge density is denoted with σ and depends on U_{int}.

We put this expression into 3.36:

$$\mathbf{j}_{2\parallel} = -\frac{iq_e\mathbf{E}_\parallel}{4\pi m\omega}\nabla\cdot\Big(\frac{4\pi(n_0(\mathbf{r}) + n_s(z, \sigma(U_{int})))q_e^2}{m\omega^2}\,\mathbf{E}(\mathbf{r})\Big) \tag{3.39}$$

Now, we can see that,$\mathbf{j}_{2\parallel}$ depends on $\sigma(U_{int})$. When the total surface charge changes, then the parallel SH current component should change proportional. The same is true for $\chi^{(2)}$ which is a macroscopic quantity. To show this in a strict manner, further calculations would be necessary, which is beyond the scope of this thesis.

So we conclude in a hand-waving manner:

$$I_{SHG,\mathbf{j}_{2\parallel}} = I_{SHG,\mathbf{j}_{2\parallel}}(\sigma) \quad \text{since} \quad \mathbf{j_2} \propto \mathbf{P^{(2)}} \propto \mathbf{E}_{\text{farfield}} \quad \text{and} \quad I \propto \mathbf{E}\mathbf{E}^* \tag{3.40}$$

This shows that there should be some sensitivity to the (electronic) surface charge of the metal, when it comes to surface SHG. This surface charge can be altered by adsorption of ions for example.

The normal surface current should depend on the surface charge too, but the derivations are much more involved.

3.6.4 Electron Spillout

In the section before about the free electron gas, we concluded that the electronic surface charge of a metal should influence the surface SHG response of a metal. Metals always have electrons reaching into the space above the surface. This electronic charge density influences the (hyper) polarisablility of the surface. When negatively charged ions adsorb at the surface, then they displace the electrons at the surface and reduce the electronic spillout, which in turn changes the hyperpolarisablility of the surface and therefore the SHG response.

3.7 SBHM Calculations

In some wavelength ranges, the SHG response of single crystalline Cu could (at least in principle) be described by the Simplified Bond Hyperpolarizability Model. Therefore, the following section contains some calculations, which acknowledge this possibility.

On a very high level, the SBHM model of surface SHG captures many important basic aspects. Electrons swing along the bonds of a solid only and experience some nonlinear force, which is characterized by the hyperpolarizability parameter, which describes how much a potential deviates from harmonicity an therefore contributes to SHG. In the SBHM, changes in the SHG efficiency of a

material (like silicon) are a geometrical effect (other effects are not considered in the SBHM). Such changes happen, when the sample is rotated like in RASHG[15] measurements.

In our case the sample is not rotated, but the applied voltage is scanned in a linear fashion. Thus, a change in SHG efficiency cannot be described in terms of geometry. The change in SHG is due to a change of the average hyperpolarizability of the interface. This could be due to a change of the number of "SHG-active" molecules/ions at the surface (a.k.a. adsorption) or due to some "intrinsic" change of the surface properties (electron spillout or gradient of the electric field or ...).

The set of the 12 normalized bond vectors which point from one Cu atom to its nearest neighbours is given by:

$$\{\hat{\mathbf{b}}_{fcc}\} = P_c\left\{\frac{1}{\sqrt{2}}\begin{pmatrix}\pm 1\\ \pm 1\\ 0\end{pmatrix}\right\} \tag{3.41}$$

Here, P_c denotes the permutation of the 3 coordinate entries of each vector(s). In Fig. 3.5, the Cu(110) surface can be seen. With a little bit of thought one can come up with the normalized bond vectors which point from the central atom to it's neighbours by rotating 45 ° around the z-axis and then rotating 90 ° around the x-axis:

$$\hat{\mathbf{b}}_{1,2,3,4} = \begin{pmatrix}\pm\frac{1}{2}\\ \pm\frac{1}{\sqrt{2}}\\ -\frac{1}{2}\end{pmatrix} \qquad \hat{\mathbf{b}}_{5,6} = \begin{pmatrix}\pm 1\\ 0\\ 0\end{pmatrix} \qquad \hat{\mathbf{b}}_{7,8} = \begin{pmatrix}0\\ 0\\ \pm 1\end{pmatrix} \tag{3.42}$$

The first four vectors point downward and to the side (z-direction is up for reference). The vectors $\hat{\mathbf{b}}_{5,6}$ are in the plane of the surface and point to the two neighbour atoms, which are in the same surface row (see Fig. 3.5). Then $\hat{\mathbf{b}}_{7,8}$ point upwards to a possible adsorbed ion or downwards to the Cu atom directly below our surface atom of interest.

Now, we can construct $\chi^{(2)}_{D,SBHM}$ as an outer product of the normalized bond vectors:

$$\chi^{(2)}_{D,SBHM} = \frac{1}{V}\sum_{j=1}^{n}(\gamma_j^{(2)}\hat{\mathbf{b}}_j\hat{\mathbf{b}}_j\hat{\mathbf{b}}_j) \tag{3.43}$$

Above, $\gamma_j^{(2)}$ denotes the second order hyperpolarizability of each bond. For the bonds that point downwards and to the side we set $\gamma^{(2)}_{1,2,3,4} = \gamma_{ds}$, because those bonds are equivalent. For the in-row bonds in the surface plane, we set $\gamma^{(2)}_{5,6} = \gamma_r$. For the bond, that points upwards we set $\gamma^{(2)}_7 = \gamma_{CuCl}$ and for the bond, that points downwards we set $\gamma^{(2)}_8 = \gamma_d$. With that we can give an explicit form for $\chi^{(2)}_{D,SBHM}$:

$$\chi^{(2)}_{D,SBHM} = \frac{1}{V}\begin{pmatrix} \begin{pmatrix} 0 & 0 & \frac{1}{4}(\cos(2\beta)-3)\gamma_{ds} \\ 0 & 0 & \frac{1}{2}\cos(\beta)\sin(\beta)\gamma_{ds} \\ \frac{1}{4}(\cos(2\beta)-3)\gamma_{ds} & \frac{1}{2}\cos(\beta)\sin(\beta)\gamma_{ds} & 0 \end{pmatrix} \\ \begin{pmatrix} 0 & 0 & \frac{1}{2}\cos(\beta)\sin(\beta)\gamma_{ds} \\ 0 & 0 & -\frac{1}{4}(\cos(2\beta)+3)\gamma_{ds} \\ \frac{1}{2}\cos(\beta)\sin(\beta)\gamma_{ds} & -\frac{1}{4}(\cos(2\beta)+3)\gamma_{ds} & 0 \end{pmatrix} \\ \begin{pmatrix} \frac{1}{4}(\cos(2\beta)-3)\gamma_{ds} & \frac{1}{2}\cos(\beta)\sin(\beta)\gamma_{ds} & 0 \\ \frac{1}{2}\cos(\beta)\sin(\beta)\gamma_{ds} & -\frac{1}{4}(\cos(2\beta)+3)\gamma_{ds} & 0 \\ 0 & 0 & -\gamma_{CuCl}+\gamma_d-\frac{\gamma_{ds}}{2} \end{pmatrix} \end{pmatrix} \tag{3.44}$$

Here, $\chi^{(2)}_{D,SBHM}$ is rotated around the z-axis (which is also the surface normal) by the angle β (which we need later on). In the expression above, γ_r is absent, because the two bonds show exactly in opposite direction an cancel each other out.

Now, we can calculate the polarisation, the far field radiation and the intensity in the same manner as in 3.5:

$$I_{pp} \propto \frac{1}{128} E0^4 \left(4\gamma_{CuCl} - 4\gamma_d + (3\cos(2\beta)+11)\gamma_{ds}\right)^2 \qquad I_{ss} = 0 \tag{3.45}$$

The 2-fold symmetry is clearly visible. When we look at 4.1.2, then we need to set $\beta = \pi/4$:

$$I_{pp} \propto \frac{1}{128} E_0^4 \left(4\gamma_{CuCl} - 4\gamma_d + 11\gamma_{ds}\right)^2 \tag{3.46}$$

We make a further simplification and set $\gamma_{ds} = \gamma_d = \gamma_{Cu}$. This means that all the downward bond is equivalent to the 4 bonds that point downwards and to the side ($\hat{\mathbf{b}}_{1,2,3,4}$):

$$I_{pp} \propto \frac{1}{128} E_0^4 \left(4\gamma_{CuCl} + 7\gamma_{Cu}\right)^2 \tag{3.47}$$

In general, the hyperpolarizabilities are complex:

$$I_{pp} \propto \frac{1}{128} |E_0|^2 \left(4\gamma_{CuCl} + 7\gamma_{Cu}\right) \left(|E_0|^2 \left(4\gamma_{CuCl} + 7\gamma_{Cu}\right)^* \right) \tag{3.48}$$

3.8 The SHG Response of Adsorbates - A Working Hypothesis

In general, it is rather difficult to model surface SHG. There are often multiple mechanisms responsible for the SHG response of an interface. To simplify the analysis of the measurement data, some effective model that is simple enough is often required.

When we think of a clean, single crystalline copper surface in HCl electrolyte, the Cl ions can adsorb on the surface of the copper, when the appropriate electrical potential has been applied. The adsorbate layer that forms, covers the copper surface at least partially and modifies the interface in certain ways. Because SHG in reflection is very surface sensitive, it should in principle be possible to detect a change in SHG intensity or polarisation. Regardless of the exact mechanism, the SHG response of the system has several components:

- the effect of the adsorbate under investigation (especially large molecules)
- the bare copper surface and bulk, where the SHG response is governed by mostly free electrons
- interaction effects between the adsorbate and the surface.
- contributions from the electrolytic side of the interface
- interaction effects between the adsorbate and the electrolyte.
- interaction effects between the metal surface and the electrolyte.

Let us assume for simplicity, that *regardless* of the types of SHG mechanisms, that the (effective) second order electric susceptibility can be split into two parts: The first is independent of the adsorbate surface coverage and the second one is proportional to it:
In this manner[18], the χ_2 can be written as:

$$\chi_2 = \chi_{2,0} e^{0i} + a\theta e^{i\phi} \tag{3.49}$$

where a is a proportionality constant, ϕ denotes a possible phase shift between the two SHG terms and θ is the surface coverage. Then the intensity is:

$$I_{SHG} \propto \chi_2 (\chi_2)^* = \chi_{2,0}^2 + 2\chi_{2,0}\, a\theta \cos(\phi) + (a\theta)^2 \tag{3.50}$$

Which is quadratic in the surface coverage.
Now, if we only have access to the absolute value of $\chi^{(2)}$, we can write this down as:

$$|\chi_2|^2 = \chi_2 \chi_2^* = \chi_{2,0}^2 + 2\chi_{2,0}\, a\theta \cos(\phi) + (a\theta)^2 \tag{3.51}$$

and

$$|\chi_2| = \sqrt{a^2\theta^2 + 2a\chi_{2,0}\theta \cos(\phi) + \chi_{2,0}^2} \tag{3.52}$$

which gives in linear approximation for small a:

$$|\chi_2| \approx \chi_{2,0} + a\theta \cos(\phi) \tag{3.53}$$

Since the equation above is overparameterized for the fitting of the measurement results, we lump the constants and get:

$$|\chi_2| \approx \chi_{2,0} + a_{eff}\theta \tag{3.54}$$

This last equation is important for the analysis and fitting of the measurement results and intensity traces. We compare this to equ. 3.48 and get:

$$|\chi_2| \simeq 7|\gamma_{Cu}| + 4|\gamma_{CuCl}| \cos(\phi)\, \theta \tag{3.55}$$

So, with this crude calculation $|\chi_2|$ is approximatively proportional ($\simeq$) to a sum of two parts: The first part is 7 times the absolute value of the hyperpolarizability of a Cu-Cu bond and the second part is 4 times the absolute value of the hyperpolarizability of the bond between a Cu surface atom and an adsorbed Cl ion times the surface coverage times the cosine of the phase difference ϕ between the two contributions.

4 Experimental Setup & Procedures

4.1 Setup

4.1.1 Optical Part

The optical setup is largely the same as in ref[14]. In Fig. 4.1 and 4.2 the essence of the optical setup has been captured. Multiple mirrors have been omitted, as they were only guiding the laser beams. The most important part of the setup between M_1 and M_2 is depicted with correct angles: the beam impinges on the sample surface with an angle of 45°.

Laser System

The laser system consisting of a pico second laser (PL2241A-50 (Nd:YAG @ 1064 nm)) and an optical parametric generator (OPG) (model: PG501-DFG1P) is from EKSPLA. The OPG is pumped by the (H500 @ 532 nm) unit which converts a major fraction of the 1064 nm pulses to 532 nm. The H500 is "pumped" by the main laser (PL2241A-50). The OPG output is tunable in the visible / near IR in the 680nm-10μm wavelength range (for the experiments the 680-1064nm output was used) with a pulse rate of 50 Hz and a pulse energy of 0.5 mJ and a pulse duration of 30 ps.

Optical Path

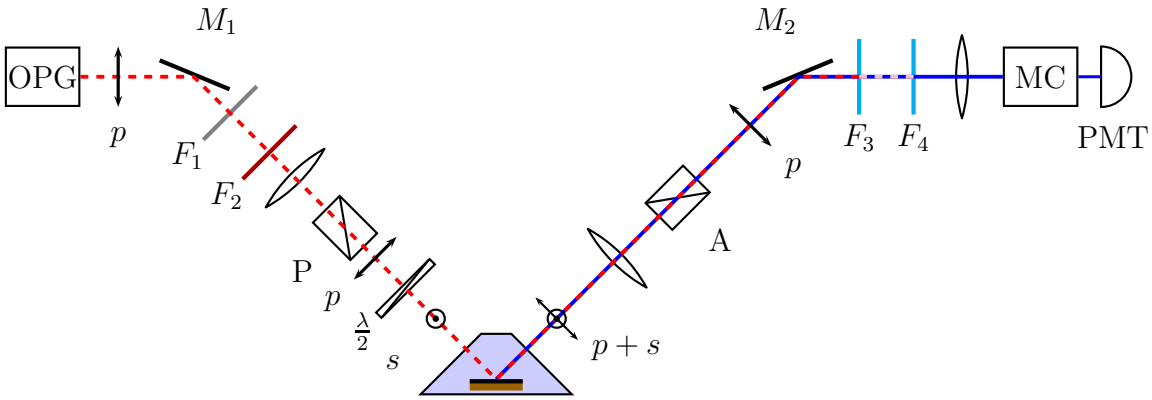

Cu (110) immersed in electrolyte cell

Figure 4.1: Sketch of the optical setup with s-input and p-output polarisations ($s = 0°$ and $p = 90°$ respective to the normal of the paper plane). Polarizers (P, A) are Glan-Thompson prisms (Glan-Laser Calcite Polarizer (Thorlabs GL10-B (with anti-reflective coating in 650-1050 nm range))). Filter F_1 is an optional neutral density filter with an optical density of $OD = 0.6$ (transmission is $T \approx 0.25$, not completely constant at all wavelengths (Thorlabs NE06B-B (with anti-reflective coating in 650-1050 nm range))). Filter F_2 is a longpass filter which transmits wavelengths longer than 645 nm (Thorlabs FGL645). Filters F_3 and F_4 are identical (Thorlabs FGB 37 (bandpass 335-610 nm)). The half-wave plate $\frac{\lambda}{2}$ has achromatic retardation and anti-reflective coating in the 690-1200 nm range (Thorlabs AHWP05M-980).

The laser pulses exit the OPG and are guided to hit M_1 via several mirrors. Along the way a small fraction of the pulse is separated off with a beam splitter an then guided to a photodiode to measure the pulse energy/intensity. Then the pulse passes F_1 (optional) to reduce the pulse intensity if needed. In principle one could reduce the pumping intensity of the OPG to get pulses of lower intensity, but for too weak pumping this can lead to unstable behaviour of the OPG.

Then the pulse passes a longpass filter (F_2) to filter out any shorter wavelengths that come from the OPG or the H500 (532 nm). Then the pulse runs through a lens to focus it onto the sample surface which comes a few optical components afterwards. After the lens the pulse runs through a polarizer prism (P) to increase the polarisation purity of the already pre-polarized laser pulse. To adjust the polarisation direction, the pulse hits a half-wave plate, which, for this purpose is rotatable.

Then the pulse enters the electrochemical cell via quartz window, travels through the watery electrolyte and hits the sample in a focused manner. Here, the SH photons are generated and travel with the reflected pulse trough the electrolyte and exit the cell via a second quartz window. Then the pulse is focused again and passes the rotatable analyser prism (A) to separate out the desired polarisation. After hitting M_2 the pulse is guided via several mirrors to two bandpass filters ($F_{3/4}$) to filter out the fundamental beam wavelength / first harmonic component. Afterwards, the pulse is focused onto the entry slit of the monochromator (MC), which is tuned exactly to the SH wavelength. The monochromator forwards the pulse to a photomultiplier tube (PMT), which greatly amplifies the pulse to enable its detection thereafter.

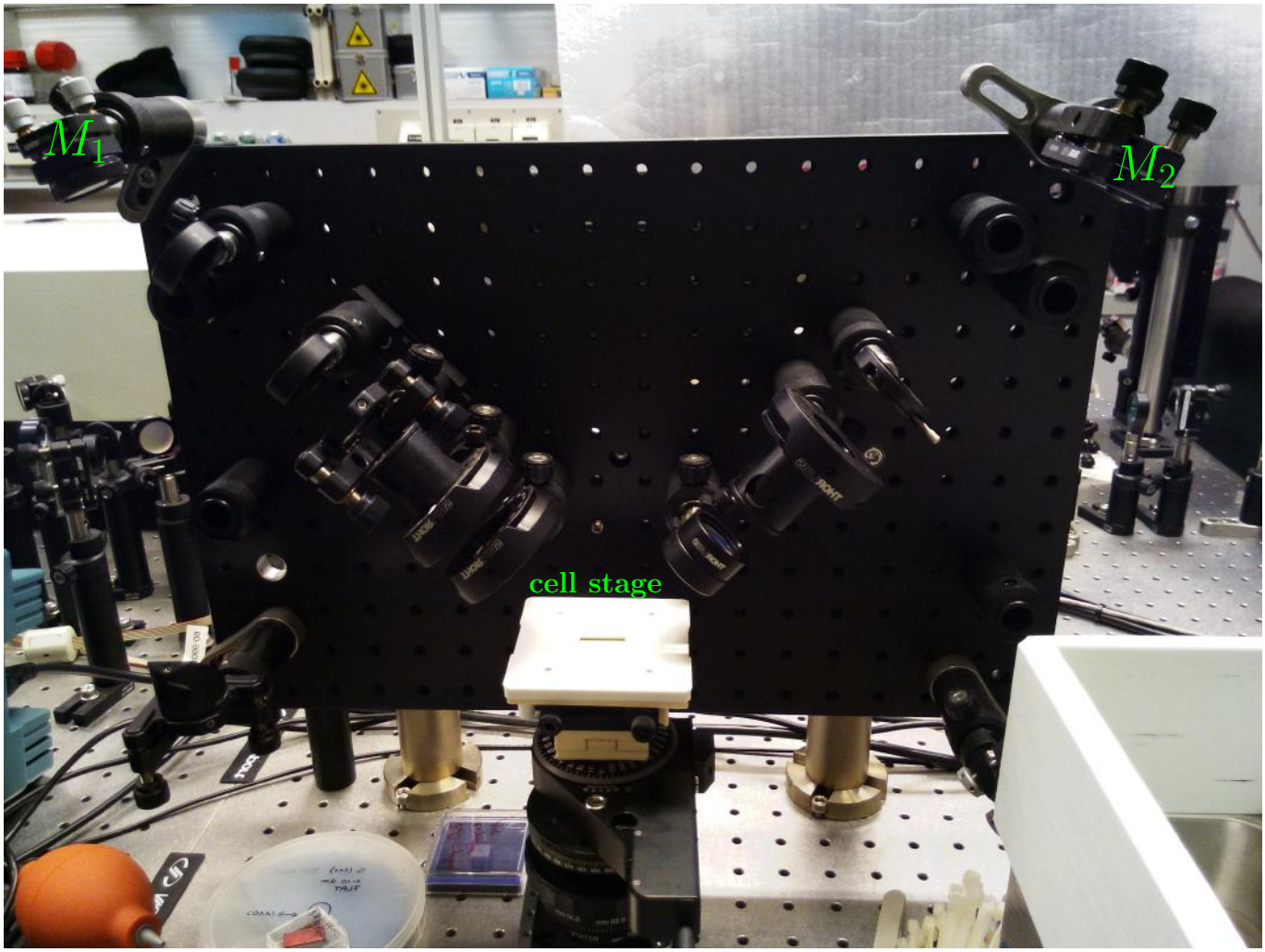

Figure 4.2: Setup in the laser lab.

4.1.2 Copper Sample

The sample used was a rectangular, monocrystalline Cu (110) sample bought from MaTeck GmbH as 1p1-type (polished on one side and a orientation accuracy better than 1°) and with 99.999 % purity.

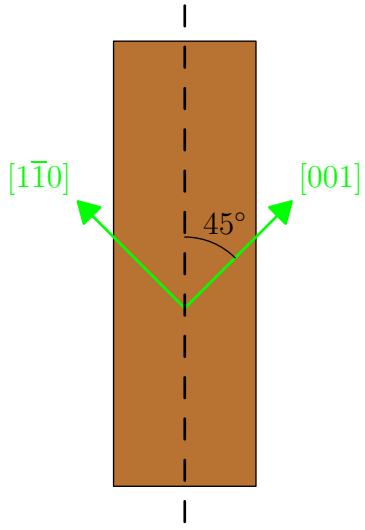

Figure 4.3: Copper (110) sample from above with dimensions of 25x8 mm and an initial thickness of 1.5 mm. The crystallographic orientation and the plane of incidence and reflection of the laser light are indicated

4.1.3 Electrochemical Setup

Electrochemical Cell

The most important part of the cyclic voltammetry setup is a cell with optically transparent windows to allow surface SHG measurements (see Fig. 4.4 - Fig 4.6). The liquid electrolyte is contained in this cell to allow the formation of an solid-liquid interface especially at the investigated sample. The body of the cell is machined from PEEK which stands for polyether ether ketone, which is a brownish thermoplastic polymer and is known for its chemical resistance and its mechanical stability. The chemical resistance is needed for the cleaning procedures which involve HCl. And the mechanical stability makes CNC milling more practical. In addition, PEEK is not extremely hydrophobic like polytetrafluoroethylene (PTFE) which is prone to air bubbles sticking to its surface for that reason.

The connection to the hoses and the electrodes are made from PEEK too. The optical windows are quartz glass discs, which are transparent in the visible and NIR range. The windows are held in place with window holders made from a suitable polymer. The holders themselves are tightened with screws and springs to the body of the cell. To prevent leakage of the electrolyte to the outside and leakage of air to the inside, the windows rest on O-rings, which are highly chemical resistant, which is needed for cleaning them with harsh chemicals (HCl).

The cell has platinum wire coil as the counter electrode in its top part below its lid and a Ag/AgCl wire running to the very bottom part of the cell. This is then the reference electrode which picks up a voltage reference near the sample surface.

The cell sits on top of the sample and is held in place by a clamp which is tightened to the base of the cell which also acts as the sample holder. This clamp and the base were 3D-printed with PLA polymer (polylactic acid).

Electrical Connections

The sample and the electrodes are connected to an IVIUM potentiostat, which has a corresponding input for every electrode. The potentionstat adjusts the voltage between the counter electrode and the working electrode (sample) in such a way that between the reference electrode and the working

electrode a desired voltage is reached. At the same time the current between the counter electrode and the reference electrode is measured. The reference electrode is very close to the surface of the sample. This enables the sensing and control of the voltage drop across the electrochemical interface with minimal interference from the voltage drop in the electrolyte, which is due to the ohmic resistance of the electrolyte.

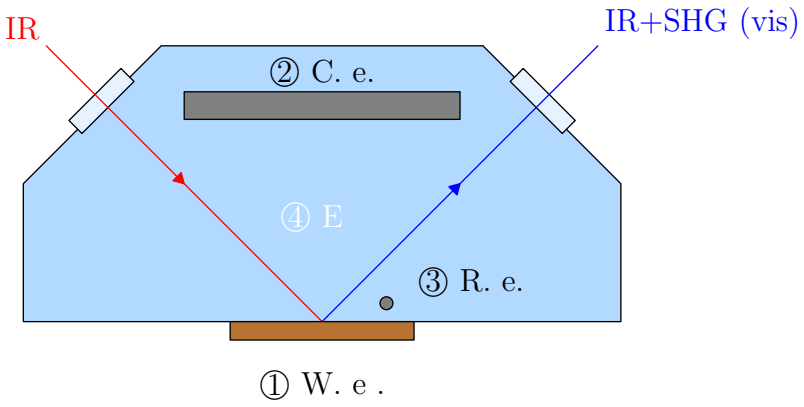

Figure 4.4: Principle of the flow cell (cross section) with fused silica windows and electrolyte indicated. 1,2 and 3 indicate the working electrode (Cu (110) sample), the counter electrode (platinum wire coil) and the reference electrode (Ag/AgCl-type). The incoming beam is denoted with IR and the number 4 is assigned to the HCl electrolyte

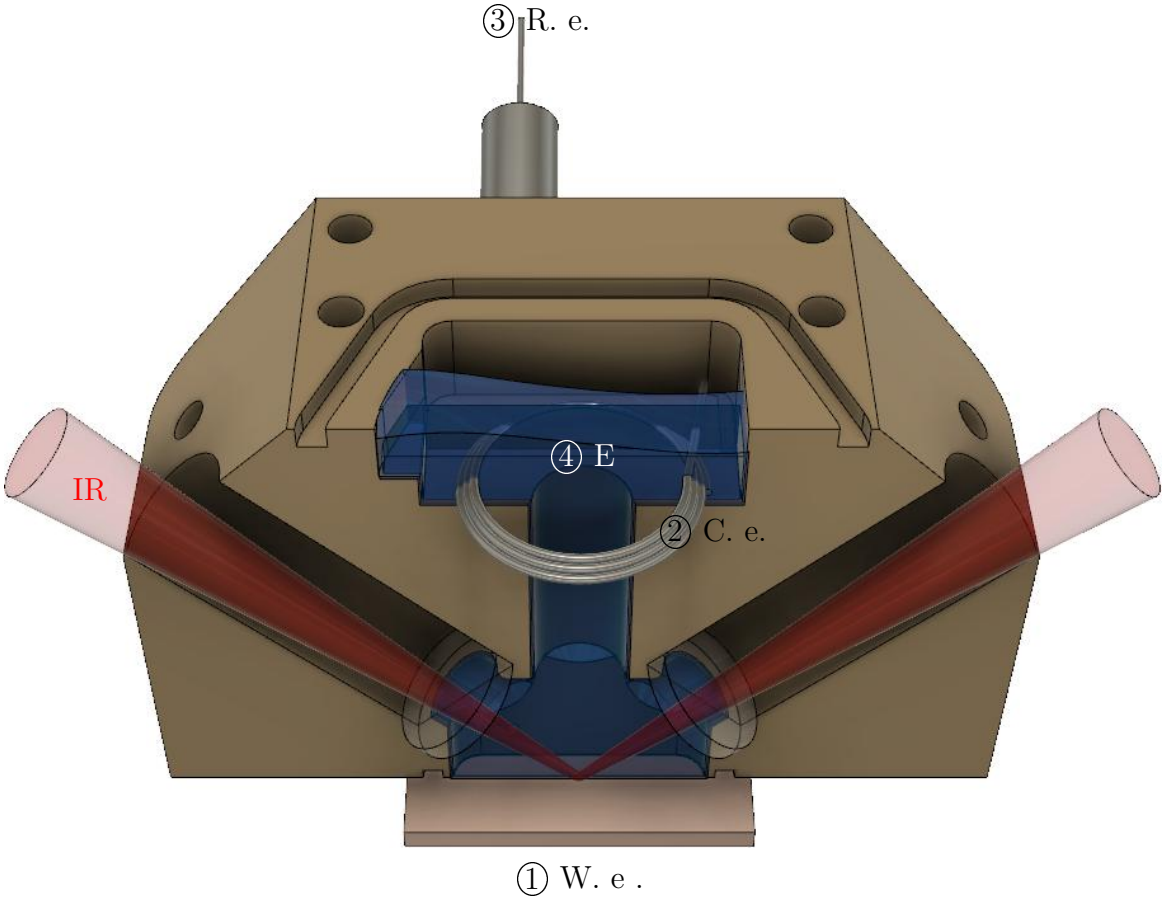

Figure 4.5: 3D model of the electrochemical cell with cut view in the plane of incidence of the laser beam. The lid of the cell has been omitted as well as the window holders. The reference electrode is a wire that runs through the hose connector all the way to the bottom of the cell and ends 1 mm above the working electrode.

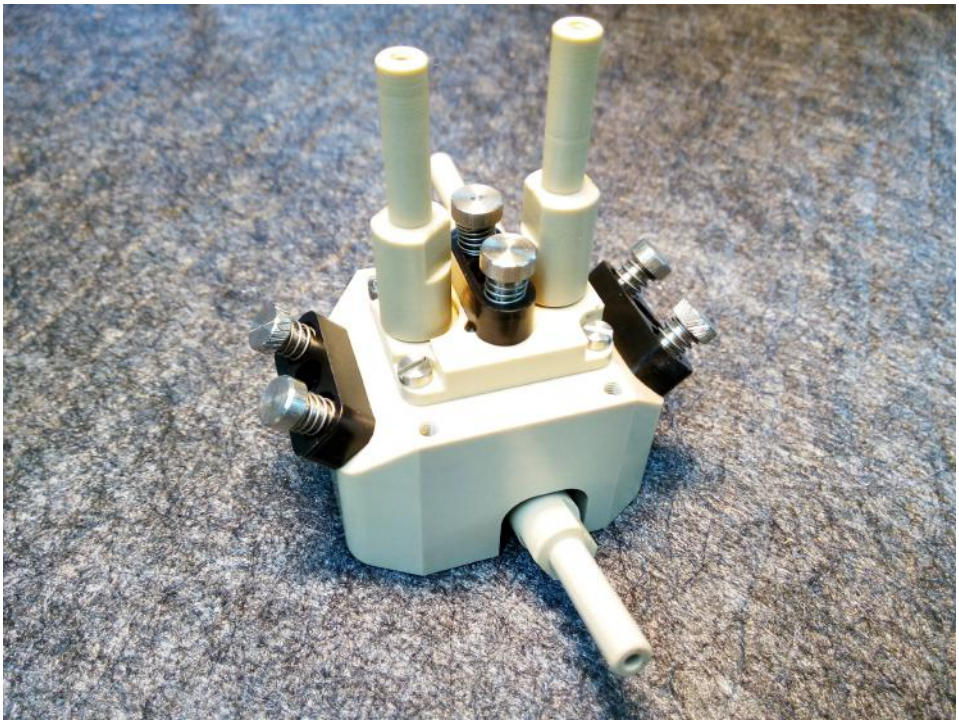

Figure 4.6: Freshly manufactured cell at the ZONA workshop (still without electrodes) with lid and window holders (black)

Chemical Part for Electrolyte Preparation

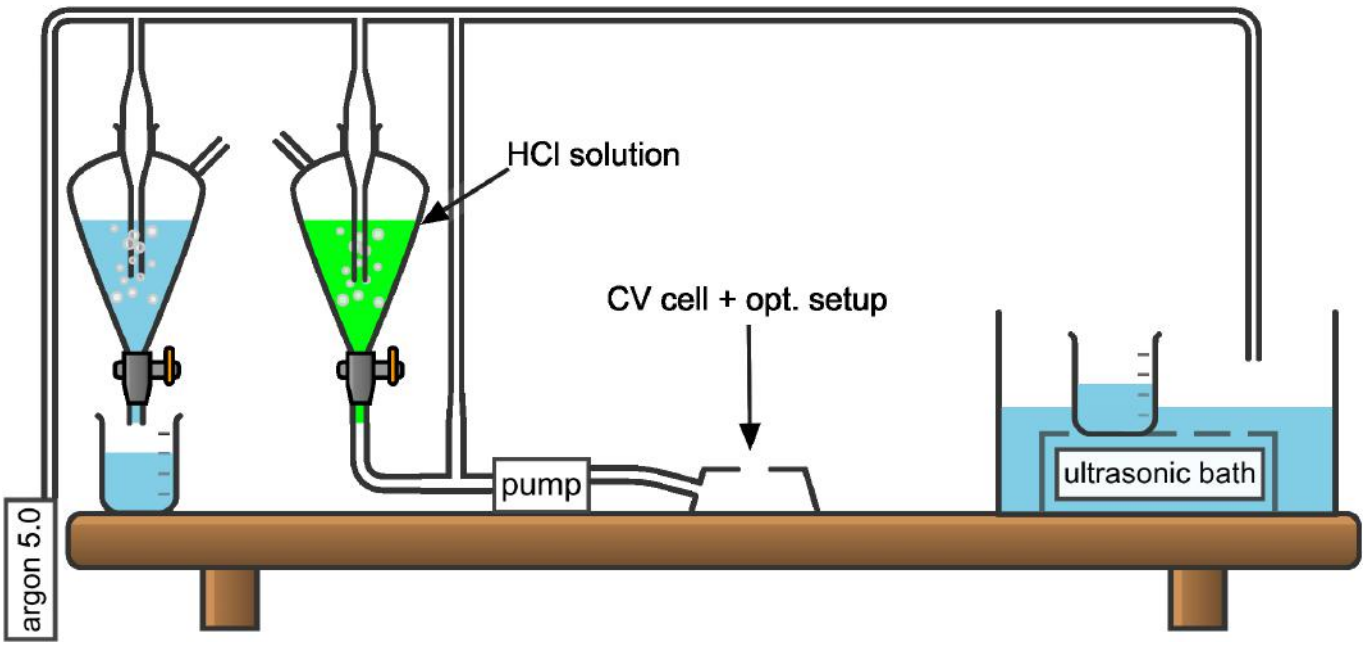

Figure 4.7: Diagram of the chemical setup: Argon gas (99,999% purity) is fed into a system of hoses to deaerate some ultrapure water (left container) as well as the HCl solution (right) by saturation with argon trough bubbling. Both containers have taps to drain the liquids when needed. The hose system topology ensures that in front of and after the column of HCl solution no air and only argon exists. The pump feeds the solution to the CV cell. In the same way, the ultrasonic bath is filled with argon to exclude air during ultrasonic cleaning.

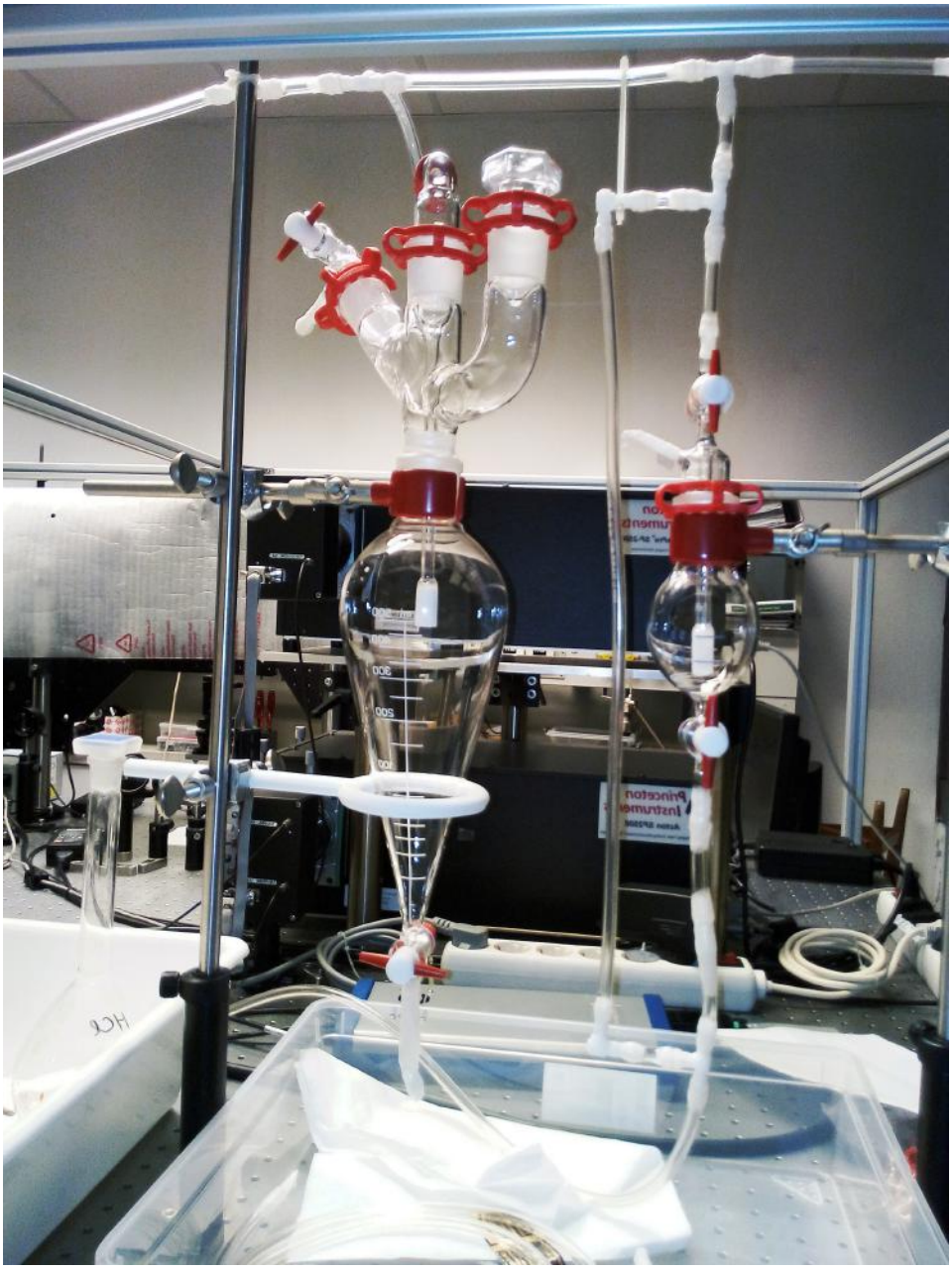

Figure 4.8: Photo of the chemical setup: The gas flow to the containers can be controlled at the top, where the gas outlet is as well. The argon enters the containers through a glass tube and gets dispersed trough a porous glass element at the end to create small bubbles, when submerged.

CAD Modeling of the Cell

This is cell has been adapted and improved to fit to the previously existing optical setup (angle of incidence). The cell for linear optical in situ (ellipsometry) and electrochemical measurements that's already in use, has a shallow, nearly grazing angle of incidence. My approach was the following: as much backwards compatibility with existing equipment as possible and an optimized design for SHG, which is not too difficult to fabricate with CNC milling. I went through quite a few iterations, to find and optimize the balance of these three requirements. This had the side effect of improving my CAD modeling skills substantially.

Backwards Compatibility I wanted to use the same glass windows as well as the same O-rings to seal the cell and the same samples, because they where in store at the lab. The inlets and outlets are the same too. This ensures compatibility with the existing pumps and hoses. The top of the cell and the lid is also the same, because there was no reason to change it. Besides, Bernhard Fragner at the ZONA workshop probably still had the old CNC-codes from the other cell.

SHG Optimized Design

The main challenge here was to minimize the length travelled in the watery electrolyte by the incoming near infrared laser pulse, as water has strong absorption in the infrared region. This was achieved by locating the glass windows as close as possible to the sample. To make this possible, the central vertical chamber was changed from a long hole to a round bore, which is smaller in size and easier to fabricate.

Air Bubbles Countermeasures The steeper incidence angle elicits increased problems with air bubbles in the optical channel, when filling the empty cell - Dr. Christoph Cobet told me. Air bubbles get trapped in the optical channel and cover parts of the glass windows. This obstructs the beam path and must be avoided at all cost. At first, Dr. Christoph Cobet and me thought of an additional channel between the electrode bay and the top part of the optical channel where the glass windows are located. This should encourage most of the air to rise to the top of the cell and to escape the optical channel in this manner. After some conversations with Bernhard Fragner from the ZONA Workshop and Dr. Christoph Cobet again, it was decided that locating the locating the glass windows closer to the sample would greatly improve the situation. The additional channels would have been quite difficult to manufacture.

Ease of Manufacturing Because the top of the cell remained unchanged, but the angle of incidence was steeper, the total height of the cell increased. This led to the problem that the central vertical chamber and the optical terminals got longer/deeper. Because both of them where long holes they had to be milled with milling tools. For standard milling tools, the diameter to length ratio is 1:3 due to reasons of rigidity and reproducible tolerances. So I changed the optical terminals to round holes which can be drilled to basically any depth. The top part of central vertical chamber, which was a long hole, was made wider, so that it could be milled more easily. The bottom part remained the same, because it had to fit the samples at the lab. In the end the top part of the chamber was replaced with a round hole too.

The air sides of the optical channels had notches to remove the glass windows and the O-rings more easily. These were omitted in the my new design, as they had to be milled quite deep and Dr. Christoph Cobet said, that those were not used much at all, because the windows were removed by pushing from the inside with a Q-tip. Tn addition, this method is better suited for the more fragile CaF_2 windows, when those would be in use.

Other Changes A special feature at the bottom, which was to contact samples with low conductivity was omitted. The position of the reference electrode, which was at the center was moved more to one side, as it sometimes blocked the laser beam. Berhard Fragner then suggested to make the electrolyte inlet at the other side of the inlet for the reference electrode wire the same, so that he can use the same CNC code twice. This was fine with Dr Christoph Cobet, as long as the special feature at the bottom could be added later. Since this was possible, I realized it.

4.1.4 Whole Setup

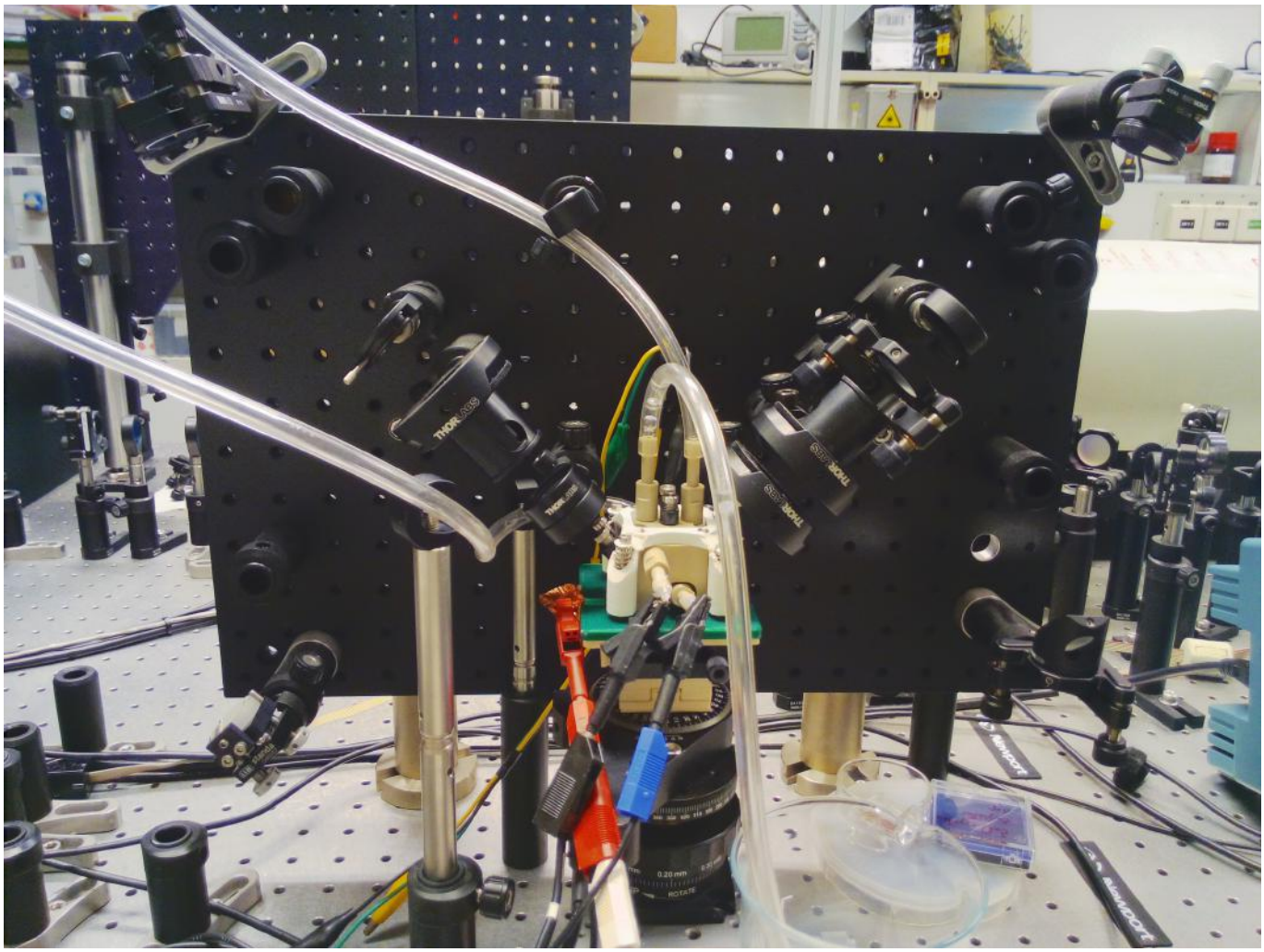

Figure 4.9: Main part of the setup in operation. The electrochemical cell is at the center and attached to the clear hoses, while the optical parts are in a 45 degree reflection type arrangement.

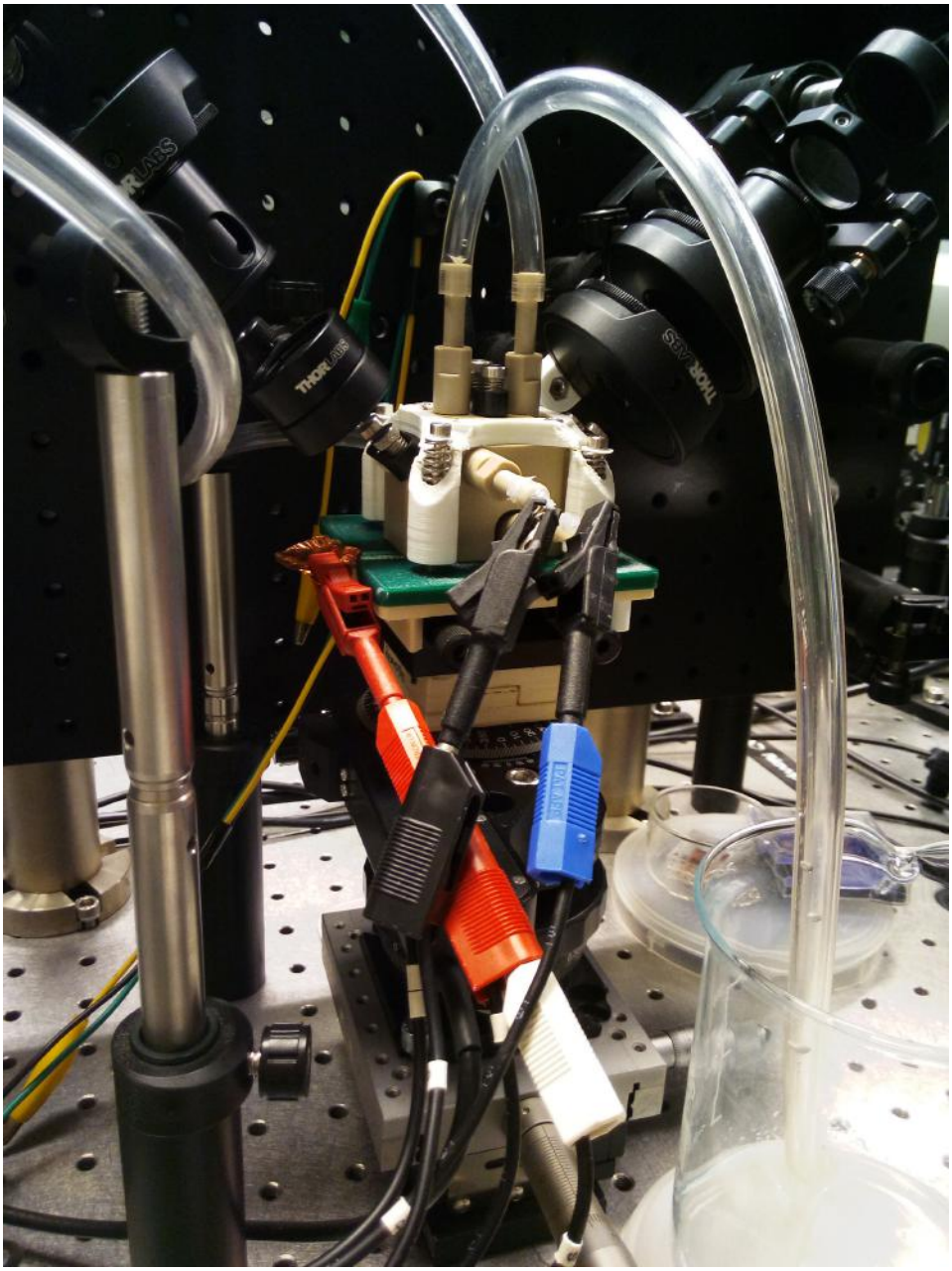

Figure 4.10: Closeup of the cell at the center: Electrolyte is fed in from the back side, argon flows into the cell at the top right connector and leaves the cell through the left connector in to the beaker. The copper foil below the cell is in electrical contact with the copper (111) sample and is connected to the red electrical connector of the W input of the potentiostat. The blue electrical connector is in contact with the reference electrode and the black one contacts the platinum counter electrode.

4.2 Milestones and Progress

One aspect of this thesis was to preserve some of the know-how necessary to run experiments in the small and until now rather dormant laserlab (the former "Christian Doppler Laboratorium für mikroskopische und spektroskopische Materialcharakterisierung"). Hence, this section contains some of the lessons learned and things that were improved or issues, that I found challenging. The most important of those are written down below, so that others can read them in the future.

4.2.1 First Cell Prototype and Sanity Check

The first prototype was made out of a cheaper material than PEEK (polyether ether ketone), to get the CNC milling right and to make a first system check. After it was milled, I said to Berhard Fragner, he should finish it completely by also cutting threads into holes so that it could be assembled properly. He agreed reluctantly and argued that the material it too soft for threads to be stable. However, they were stable enough to conduct first watertightness tests. Those showed no leaks, after we used the right O-rings for sealing. This prototype had no problems with air bubbles in the glass windows. After that, it was mounted in the beam path of the SHG setup without water inside and with the glass windows. As a temporary sample, an old Si (111) wafer fragment was used. It was possible to get an SHG signal. Then the improvised pump was turned on to fill the cell with deionised water. As anticipated, the SHG signal vanished at first and then recovered a bit as the cell was filled. Some beam path alignment was necessary, to correct for the longer optical path length in the water inside the cell, which causes the laser focus to shift upwards a bit. Or more precisely: The longer optical path in water causes the laser focus to shift against the beam propagation direction. The result is that the laser focus moves away from the surface, which diminishes the SHG signal.

4.2.2 Cheaper Platinum

For CV (cyclic voltammetry), a platinum wire was needed. Platinum is expensive and lab-grade purity platinum is way more expensive. So the price on the world market was around 26 €/g. The last order of 99.9 % purity platinum from a lab supplier came at a cost of around 140 €/g with VAT (value-added tax). This is more than 5 times the price than regular platinum for investment purposes. Understandably, I wanted a cheaper source of platinum. Dr. Christoph Cobet said to me, that this is okay, as long as the purity is the same or higher than the purity of the platinum wire, that was ordered in the past. It was hard to find a cheaper source of lab-grade purity platinum from lab suppliers online. After the realisation, that platinum belongs to the precious metals like gold and silver, a quick online search led to a supplier of precious metals, which also sells semifinished products to goldsmiths and watchmakers. This supplier (R. Götze GmbH & Co. KG) is a refinery of precious metals as well. Luckily, they had some 99,95% purity platinum wire at low price: 42,5 €/g for business customers, which is less than one-third of 140 €/g. So 1 m (4,22 g) of this platinum wire with a diameter of 0.5 mm was ordered.

4.2.3 Software Issues

At the beginning of the Spezialpraktikum, the laser system had some software troubles. Those where mainly connection problems. LabVIEW did a bad job at connecting to the laser setup and the rotational stage. I bypassed this by controlling the rotational stage from Python and by using the automatic log files with timestamps and the intensity data of the live monitoring program, which is used only for alignment, to get angle resolved intensity measurements. The actual measurement program is not working to this day.

A look at the old LabVIEW programs (written by DI.in Cornelia Reitböck) revealed, that LabVIEW was mainly calling C-functions from .dll files to control the laser and to read intensity data from the photomultiplier and photodiodes. So it shouldn't be so hard to do this in C/C++ or better Python (Python is much easier to program than C/C++ and there are lots of software packages available that are easy to install).

Python Programming - Towards a New Laser Measurement Software

So I started to write the core functions for retrieving intensity data from the laser setup by using the *ctypes* module in Python, which enables the import and use of functions from .dll files (dynamic-link libraries), that came with the laser software. To my surprise this worked, but there was no connection to the laser. Since the issue was not extremely pressing, because my workaround at that time was working and measurements were possible, I tried again after some time and found out, that additional files which handle the USB/RS-232/CAN-Bus connection were needed. Then everything progressed really neatly by doing some trials and errors and by looking at the old LabVIEW files and consulting stackoverflow.com (online community of developers).

During testing and troubleshooting the new software, something caught my attention: in earlier measurements, the actual sampling rate was lower than 50 Hz, which is the rate of the pulses of the laser system. It was something like 48 Hz. So some data points had different/shifted timestamps for the SHG- and fundamental intensity. Somewhere some data has been lost or not retrieved. This is probably the fault of LabVIEW, because the execution order of a VI (LabVIEW program) is not properly defined, as it would be in a Fortran or a Python program. So, in LabVIEW, functions are executed, as soon as the inputs are determined. The VI was written in a way, that SHG- and fundamental intensity data were retrieved at the same time. This may lead to a conflict as only one of them can be executed at a time.

Fortunately, this has only a negligible effect on the past measurements. Even if there are 30% of the SHG/fundamental intensity data points corrupted in the sense that they are shifted in time by 1 pulse cycle, the outcomes do not change significantly, if the corrupted data points are not considered. The measurement data can also be retrieved relatively unaffected by only using the corrupted/shifted data points. This should not be surprising, as the angular/electrochemical scan rate is slow, when compared to the pulse rate. There is a small impact on the per pulse normalisation, which is probably noticeable as a change in the noise pattern in the unaveraged intensity curves.

Potentiostat

There are 2 Ivium Technologies CompactStat.h devices in the solid/liquid lab at ZONA. Only one of them is needed for measurements. The CompactStat.h can be controlled with the IviumSoft program which has a GUI (graphical user interface). This is nice, but there is one problem with this software: It is NOT possible to save a timestamp with every data point. This would be very convenient and important when fusing the data from CV and SHG, because every uncertainty in the CV starting time translates into a proportional uncertainty in the applied potential at a given point in time. But the CompactStat.h has a software development driver and an accompanying .dll which gives the inclined programmer control of the instrument. I used this to create a program that controls the potentiostat for CV and the laser system for the SHG measurements simultaneously. The measurement data is displayed in real time, which is not completely trivial to do in a way that simple and has good performance and does not interfere with the data acquisition. To accomplish this, multiple threads/processes (parallelisation) are used. Unfortunately, this program is not yet in use, because it seems rather buggy. Therefore, my method of choice for the future is using a program which can schedule mouse clicks with near millisecond precision to start the CV scans.

4.2.4 Final Cell Testing - Air bubbles

The final 2 cells were unlike the first prototype made of PEEK. With those some basic checks for water tightness were performed. I repaired an old peristaltic pump for pumping water which had only one pumping speed. This speed was too fast and created air bubbles in the optical path. So

the switch back to a cordless screwdriver as pump motor was made. This way pumping can be done very slowly and when the tubing is completely empty this seems to work. It does not work, if the tubing is not completely empty and therefore a mixture of water and air is present. Even a very thin layer of water that looks like a soap film creates disturbances, that lead to bubbles.

4.2.5 SHG from an Amorphous Copper Sample

As a simple check, the cell was filled with ultrapure water and mounted in the SHG setup. After some basic beam alignment, some SHG intensity from the dirty and untreated amorphous copper sample could be detected, which was a little bit surprising.

4.2.6 Pump Woes

There where 3 pumps at the at the ellipsometry lab for pumping electrolytes:

- an expensive one, that worked (I)
- a cheaper one with a dead electronics (II)
- an old one with broken pump head but working motor (III)

For starters, I made a coupler on the 3D-printer to drive the pump head (II) with a cordless screwdriver, which worked good enough at the start. After that, a two piece coupler to drive the pump head (II) with the motor of (III) was designed. This was running too fast, so some reduction gears to drive the pump 10 times slower were added.

4.2.7 Quick Assembly Clamp

After the first technically successful measurement without considerable oxidation of the copper sample, one of my conclusions was that a new method for fixing the cell on top of the sample was a good idea in the sense that it needs to be assembled quickly to prevent oxidation and air contact as much as possible. The best solution that came to my mind was a simple clamp with a shoulder and alignment pins. This clamp is held in place by screwing a threaded ring on top of it, which presses down the shoulder and therefore the clamp and the cell.

4.2.8 SHG Spectrum

Since I wrote a python script to record SFG spectra too, it was straightforward to modify for SHG spectra. Then a coarse spectrum was recorded from Cu (111) in ultrapure water with no electropolishing (surface is for sure oxidized). The SHG intensity is the strongest in the 840 - 960 nm range due to a few factors: The OPG intensity is the highest in this region and drops off especially towards the VIS/red. At the other side towards 1000 nm, the absorption of water kicks in. Furthermore, the dispersion of the refractive index of water and fused the silica windows may play a role in defocusing the laser spot slightly at the sample surface as the wavelength changes. Similarly, the size of the focal spot depends on the wavelength. So 900 nm is a good wavelength in general for getting high SHG intensity. Interestingly the SHG intensity seems to increase at 1050 nm, but this is probably an artefact of the cooling system: It causes the OPG intensity/beam direction to fluctuate (described later). The fluctuation of the beam direction becomes more and more apparent the further the beam travels: The OPG intensity measurement shows not a lot of oscillations, while the SHG intensity shows 3 peaks at 780 nm, 800 nm an beyond 1050 nm.

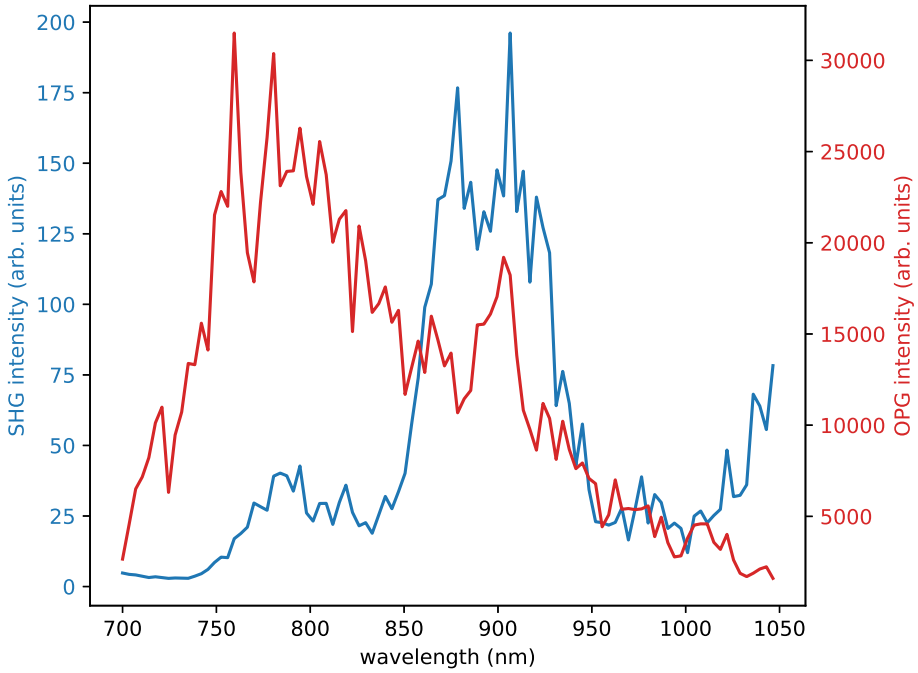

4.2.9 Migration to Windows 10

Once upon a time, USB - hub was plugged (by myself) into the Windows 7 PC in the lab, which controls the setup. This ended up in corrupted drivers, due to automatic driver installation and Windows being Windows. SHG measurements wer still possible, but not SFG measurements, since the connection to the OPG and the reference monochromator was lost in the sense that they could not be controlled from the PC any more. Luckily, the OPG has a physical control pad for setting the wavelength. Unfortunately, the System Restore in Windows 7 did not work. So, I decided to install all the drivers for the laserlab on another PC to get everything working again. After several failed attempts on my side, the support helped me to install the necessary drivers for the monocromators on Windows 10. Luckily, the OPG and the laser were easy to install. In the Python measurement scripts, pyVISA (Python package for the Virtual Instrument Software Architecture (VISA)) was dropped, because it was buggy and added no value over direct communication with the monocromators and the OPG over pyserial (Python package for the serial port) for just setting the wavelengths. After several days of computer purgatory, everything was working again (LabVIEW was not installed any more, because it was not needed).

4.3 Initial Cleaning Procedures for the Setup

In this section, some of the know-how for getting a super clean electrochemical setup (which is of paramount importance) is written down. Some of the procedures are necessary only from time to time and therefore it is a good idea to have a written record of the most important details of the different procedures and their staged execution. It is quite easy to ruin many hours of cleaning efforts merely in seconds by one or two wrong actions.

4.3.1 Cleaning of Laboratory Glassware

For deaeration of the electrolyte solution / water, the setup features two glass instruments, which are akin to gas washing bottles. Those made a trip to the glassblower (Günther Mausz), because

some adjustments where necessary. After that, some deep cleaning of the glassware was necessary.

Piranha

The glassware was cleaned with piranha solution, which is a powerful oxidizing agent. It removes most of the hard to clean organic residues. The glassware has to be reasonably clean beforehand or the solution will boil too much.

In our case we used H_2SO_4 (nearly 100 %) and H_2O_2 (30%) with the volume ratio 3:1. This means 3 parts of H_2SO_4 and 1 part of H_2O_2 are used.

Safety

It is very important to wear safety goggles, a lab coat and special long gloves. To avoid any inhalation of acrid fumes all of the procedures have to take place under a fume hood. The glass door of the fume hood should not be opened and closed with the fingers, instead use the the elbows or the heels/backs of the hand.

After every manipulation of the H_2SO_4, the neck and the orifice of the bottle has to be wiped with paper towels. After every manipulation of the H_2SO_4, the H_2O_2, the piranha solution or the wetted glassware one has to check his/her gloves if there are any drops of the said liquid. If there are some, the hands must be submerged into the water in the tray (described below). After that, the hands/gloves are dried with paper towels. The towels themselves need to be drenched in water in the sink to dilute any possible acid contamination, before they can be thrown into the trash bin.

Preparation of Piranha and Cleaning

At first, one has to pour 3 parts of H_2SO_4 into a large enough glass beaker. This glass beaker should be placed in a large, shallow plastic tray with 1-2 cm water in the tray. Then, very carefully 1 part of H_2O_2 must be added by pouring it very slowly into the sulphuric acid. The mixing reaction is exothermic. The solution gets very hot and some fumes are visible. Small bubbles should form in the solution like in soda water. The next step is to submerge the glassware carefully in the solution. After that one has to wait for 60 minutes or until no more bubbles form on the surfaces of the glassware. After 30 minutes check the solution for bubbles. If the solution itself stops bubbling, then more H_2O_2 has to be added. If one part in the initial 3:1 mixture is 500 ml (total amount of piranha is then 2000 ml), then 100 ml of H_2O_2 needs to be added.

Large Glassware

If amount of the solution is not enough to submerge the glassware completely, then flipping the glassware can do the job. To flip the glassware, one needs a beaker that is the same size as the one with the piranha solution. This beaker needs to fit into the tray too, which has 1-2 cm water in it. This container needs to be filled with ultrapure water at the same level as the piranha solution. Before flipping the glassware, one has to lift them out of the piranha solution, hold them until everything is empty and no drops fall off any more. Then the glassware goes into the ultrapure water for 5 minutes. After that, it is safe to flip, as the piranha on the glass surface has been diluted. Add 100 ml H_2O_2 again.

Then everything has to sit again for 60 minutes or until no bubbles emerge from the surfaces.

If this still does not cover the entire/desired surfaces, one can prepare more piranha in a smaller beaker and pour it over the desired spots several times after the flipping process and repeat this after 30 minutes.

Cleaning the Glassware from Piranha

After that, the glassware has to be submerged in the beaker with ultrapure water again.

The glassware can be filled and shaken with deionized water. Also the outside needs to be rinsed. This needs to be repeated 2 more times with ultrapure water.

Then the glassware is submerged in a beaker with fresh ultrapure water. The beaker is placed for 10 minutes in the ultrasonic cleaning bath. This needs to be done 3 times. If the glassware is large, then it needs to be flipped without changing the water. This would amount to 3 times 20 minutes of ultrasonic cleaning in that case.

After that, the water can be shaken off the glassware. Then it should be left to dry on paper towels and covered with the same.

Piranha Disposal

To dispose of the piranha solution, it should be poured very slowly into a acid resistant sink, while the tap water is running as much as possible. Be careful, so that there are no splashes.

4.3.2 Cleaning of Polymer Parts

Polymer parts like the cell (PEEK) should not be cleaned with (strong) piranha because this would dissolve the cell completely, but they can be cleaned with detergent and water (only if very dirty / oily from workshop), then acetone, then isopropanol, then HCl (optional) and ultrapure water. With each solvent/cleaning agent, the parts are immersed and then put in the ultrasonic cleaning bath with the beaker for several minutes (3+). This is done 3 times for each solvent (using fresh solvent every time), before doing the next stage of cleaning with another solvent. Each solvent has its own cleaning baker, which is only used for that solvent.

Cleaning the Hoses

The hoses needed for the setup require some cleaning, especially the part that are in contact with the electrolyte. To achieve this end, HCl solution (50-100 mM) is fed through the hose. Both ends of the hose are submerged in a beaker with the solution and the solution is pumped for 2-3 hours with a peristaltic pump through the hose in a closed loop. After that, the hose is emptied, blown dry with nitrogen gas and closed with parafilm.

4.3.3 Cell Cleaning and Assembly

When all the parts are clean, some assembly is required to get the cell operational.

Cleaning of the Platinum Wire

The platinum wire needs some cleaning before it is inserted into the cell. This can be accomplished by holding it to the flame of a blowtorch until the wire begins to glow brightly. The wire does not melt due to the high melting point of Pt (1,768 °C). The flame and the heat should burn all organic contaminations on the wire surface. After some cooling, the other end of the wire can be heated. The wire should be held with heat resistant pliers (metal pliers).

Insertion of the Electrodes

The reference electrode and the counter electrode need to be inserted into the cell. The counter electrode (platinum wire) is coiled up into a coil of 2-3 turns which diameter fits the top electrode bay. The end should stick out the electrode connector piece. Then the remaining orifice is closed with hot glue. This requires several attempts with hot glue, as it can be leaky, even if the glue looks like it seals the gap.

The reference electrode wire (Ag/AgCl -type) is inserted in a straight manner into its canal. It should be as close as possible to the bottom edge of the cell without ever reaching it, or else it would short circuit the potentiostat. In practice this means approximately 1 mm above the edge. The reference electrode is also sealed and fixed to the electrode connector with hot glue to make the cell watertight and to fix the electrode in place.

4.4 Experimental Procedures

4.4.1 Experimental Workflow Overview / Important Procedures

Things that are necessary:

- repeated (ultrasonic) CLEANING is necessary to keep the sample clean and to keep residues from "dirtier" preparation steps out of the clean and ultra clean steps, as the chemicals involved are sometimes quite expensive and polluting the setup will result in a major downtime. Moreover, right before the experiment and after electropolishing, cleaning of the Cu sample is done in argon atmosphere to prevent oxidation.

- To get a macroscopically flat and rather unwarped sample surface, that is suitable for reflection measurements, mechanical polishing is employed. Once in while this is necessary, because after several experiments, which include electropolishing, the sample can develop some "bumps", as electropolishing smooths the sample only locally.

- electropolishing is used after the mechanical polishing to achieve a mirror like finish of the sample, as the mechanical polishing process gives a shiny, flat sample with a slight haze. After mechanical polishing, the surface layers are for sure deformed by the pressure that the grains of the sanding paper exert on the material to remove the topmost of it. Therefore, those layers have to be removed.

  The sample gets electropolished too before every experiment to remove any surface oxidation and contamination.

- Deaeration Procedure: The electrolyte needs to be free of oxygen, as this would destroy the experiment immediately through surface oxidation. Besides, some deaerated water is necessary for cleaning after electropolishing.

- a warming up period of the laser for 30-60 min is necessary to achieve stable operation. This can be done while the dearation/electropolishing happens.

- alignment/realignment of the laser beam to direct it into the monochromator.

4.4.2 Mechanical Polishing

The sample is glued with a thermoplastic glue (CRYSTALBOND 590) to a metal (stainless steel) cylinder, which is then placed inside a guiding ring. Both are then placed on the polishing machine on the rotating 4000 grit SiC - 4000 grinding paper for wet grinding. To ensure proper polishing, the sample holder and the guiding ring must be firmly pressed against the rotating grinding paper. It is required for the sample to be continuously rotated during the polishing process to achieve an even surface finish. A small stream of water has to flow over the disk at all times. The polishing is started with slower rotation speeds, which remove material faster. Every few minutes or less, the sample should be checked visually. If the surface is flat enough, polishing is continued with a faster speed, which makes less visible scratches to the sample. The sample than can be checked with a laser pointer. If the reflection is good, then the polishing process is finished. The sample is removed from the cylinder an cleaned afterwards.

4.4.3 Electropolishing

To get a very smooth and mirror like copper surface, the sample is polished mechanically and then the sample is etched electrochemically in superpure phosphoric acid. This smoothes the surface even further. The surface dissolves slowly and the microscopic protrusion dissolve faster than the rest of the surface. Hence the surface is smoothed out and any surface contaminations are removed. Another advantage is that eventual mechanically deformed surface layers (caused by mechanical polishing) are removed.

4.4.4 Prewetting

Even with the improvements mentioned, the cell is still prone to air bubbles sticking near the windows. Saul Vazquez Miranda M.Sc. showed me his remedy for this, which is very simple: putting a droplet of the deaerated electrolyte in the position, where the bubbles stick (prewetting), before the cell gets fixed onto the sample. This works well most of the time, after some practice and 1-3 attempts.

4.5 Deaeration Procedure

The removal of air is achieved through the use of glass vessels that are similar to gas washing bottles. The electrolyte and the ultrapure cleaning water are deaerated by washing out the air with argon 5.0 (99.999 % purity). The argon bubbles 1-2 hours prior to the experiment through the liquids and takes all the air with it as it saturates the liquids and leaves the system. Also the argon is flowing in the tubing system the whole time before and during the experiment.

4.6 Experiment

When the sample is sufficiently well prepared, an experiment goes like this:

- start the laser and the deaeration procedure, by checking if enough electrolyte and ultrapure water are in the vessels of the setup and by turning on the argon flow from the gas bottle.
- start the electropolishing procedure and let it run for 10 minutes at least.
- transfer the sample to the prepared beakers with deaerated ultrapure water in the ultrasonic bath with argon atmosphere.

- clean the sample with ultrapure water 3 times in this bath
- transfer the sample with a large drop of deaerated water on top onto the sample holder as quick as possible
- put the cell which has already argon flowing through it on top and fix it with the clamp.
- fill the prewetted cell very slowly with electrolyte and check if the optical path is free of bubbles.
- check if the sample preparation was good, by running a few CV cycles.
- put the cell with the base onto the sample stage and align the beam path, such that there is a strong detectable SHG from the sample.
- start the CV scan and the data acquisition for the laser at the same time
- let the experiment run as long as desired (one may switch the polarisation and do a realignment of the laser beam) or until the CV gets bad due to oxygen leaking into the system or other undesired effects.

5 Measurement Results

5.1 Measurements

Proof of (Technical) Principle

The very first measurement(s) suffered a lot from surface oxidation, because the clamp was not fixed properly and there was some leakage. We had to remove it several times, which caused a lot of oxygen to enter the system, even with argon flowing over the sample, while removing the screws.

There is Something but What?

In general, the intensity data (see Fig. 5.1) are very noisy (more about that later). So it is basically next to impossible to assess whether a measurement is successful or not, while the measurement is running. Although the intensity data is displayed in real time in the python measurement program, the noise in the intensity masks a possible change of the Surface SHG signal during the CV cyles.

Another measurement (see Fig. 5.1) with an acceptable CV resulted in some interesting measurement data: The FFT (see Fig. 5.3) of the SHG intensity showed a peak at the frequency, which corresponded to the CV cycle period. This is a strong indicator of a response of the SHG intensity to potential dependent surface changes.

Also the autocorrelation (see Fig. 5.2) of the intensity data showed the right periodicity and number of peaks, although quite weak.

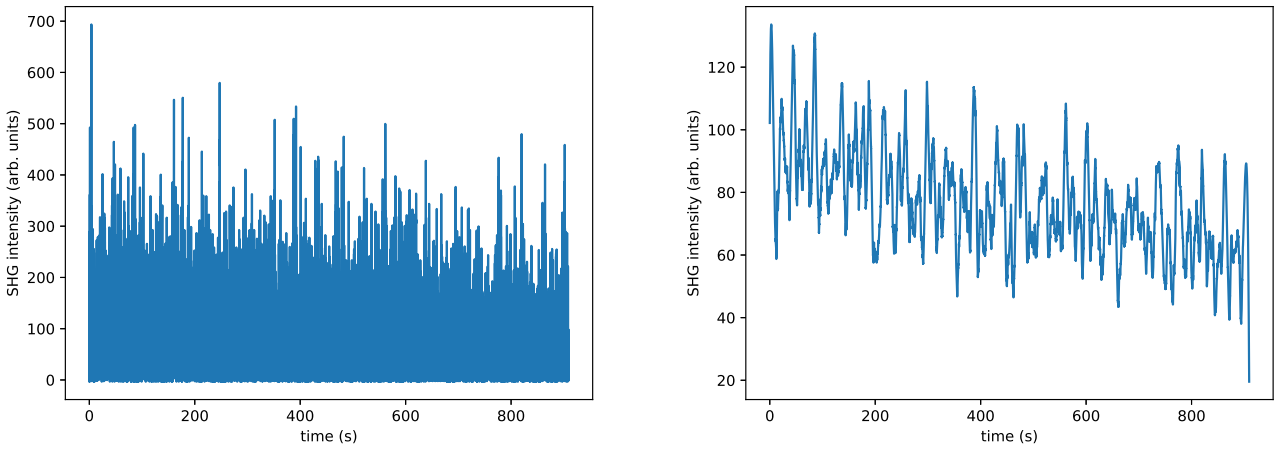

Figure 5.1: **Left:** Raw SHG intensity trace with detector background subtracted. A large amount of noise and a decline in intensity is clearly visible. **Right:** Savitzky Golay filtering over 1075 points (21.5 s) removes some noise and reveals some quasiperiodic behaviour

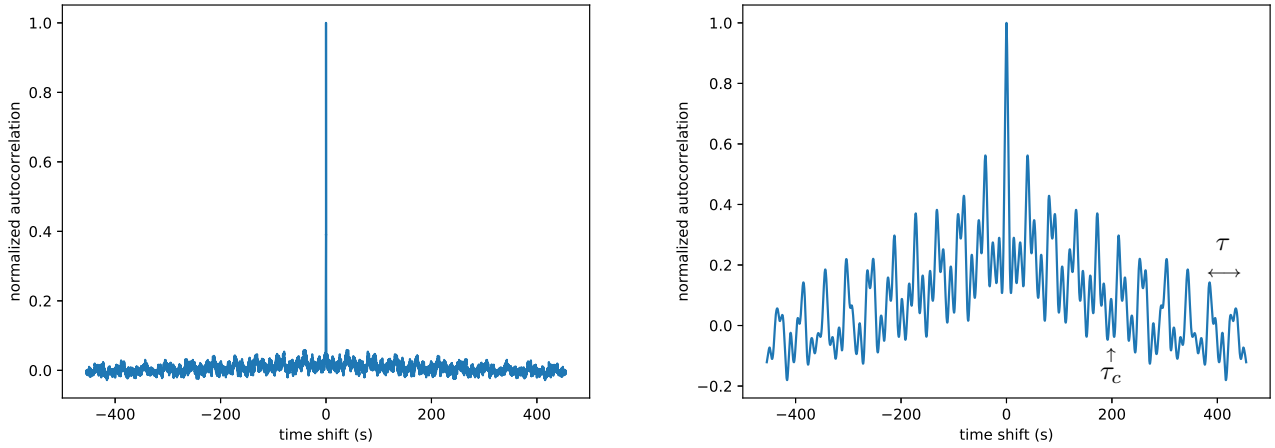

Figure 5.2: **Left:** Autocorrelation of the raw intensity trace of which the mean was subtracted beforehand. **Right:** Autocorrelation of the intensity trace of which the mean was subtracted plus Savitzky Golay filtering over 1075 points prior to the calculation of the autocorrelation. The period of one cycle is 43 seconds and indicated with τ and an arrow at the right side of the diagram between two peaks. The oscillation period of the cooling system (13 s) is indicated at the bottom with τ_c.

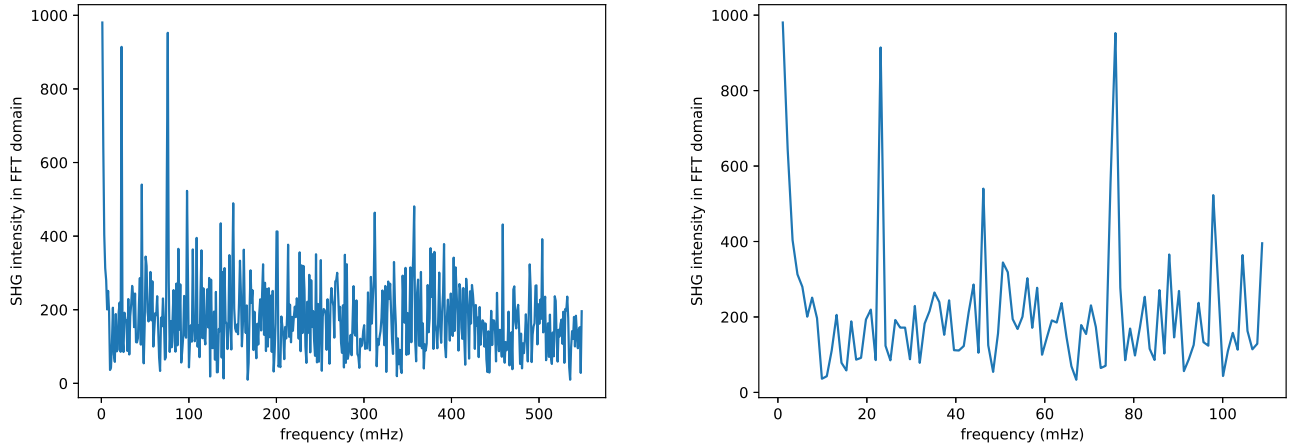

Figure 5.3: FFT amplitudes of the low and lowest frequencies of the intensity trace

Averaging over several cycles showed no clear pattern, as the noise was too strong, regardless of the smoothing procedure applied.

Further, the OPG intensity showed pronounced oscillations of 13 s duration. The cause is the cooling system of the laser which is operated by a bang–bang controller, as I found out later. This means the flow of cooling water is either on or off. By switching back and forth, the desired temperature is maintained approximately, as there is always some over- or undershoot. Better would be a PID controller which would be state of the art. This periodic temperature fluctuations drive variations in the thermal lensing of the laser crystal, which drives the intensity oscillations.

Data Analysis - Considerations

The intensity data is very noisy. The reason for this is that any fluctuations in the intensity of the pumping laser appear in a squared manner after the pulses are converted from 1064 nm to 532 nm in the H500 unit via SHG. After that, the pulses go to the OPG unit and there the pulses are converted using another nonlinear optical process to the desired wavelength. And after that we use the pulses to investigate our sample via SHG. We have 3 nonlinear optical processes in a row which blow up the noise quite a lot, as in each process the resulting intensity is proportional to the square of the incoming intensity. The main culprit however is the OPG, which not only "squares" the noise of the pumping beam but also adds 9 times the amount of noise of the pumping beam in terms of σ_I/μ_I to the output, where σ_I is the standard deviation of the intensity output and μ_I is the mean of the same.

One seemingly natural way to handle such pulse-to-pulse fluctuations in intensity is to calculate for every pulse the ratio of the SHG intensity and the the square of the incoming intensity:

$$r = \frac{I_{SHG}}{I_0^2} \tag{5.1}$$

This does not work for two reasons:

- the ratio of two very noisy traces of data is quite useless as the noise in the denominator will make things much worse, when the part of the noise, which has no correlation with I_{SHG} dominates in I_0. One could at least try to smooth the I_0 a bit, but in our case this is not helping either and it defeats the purpose a bit too, because then it is not a strict per pulse normalisation any more.
- in our case the so-called I_0 is not available. Only a measure of pulse energy is at our disposal. A less intense pulse with a longer duration can still have the same energy, but the SHG process is different due to the difference in intensity.
- there is probably some additional noise generated in the photomultiplier and the photodiodes.

Further, the intensity drops as the experiment goes on. This can be approximately repaired by dividing the intensity traces by a fit polynomial of order 2-4, which captures the drop in intensity. This is not necessary when the (lock-in style) FFT filtering method below is applied.

The cooling oscillations are well defined in the FFT and can be set to zero or reduced to the noise level, if FFT filtering is not applied.

Singularity Free Normalisation

Because of the noise in the intensity data, the above mentioned naive way of per-pulse normalisation does not work. This kind of division by the square of the incoming intensity has a singularity at zero incoming intensity: a pole of order 2. Is there some other kind of correction of the per-pulse fluctuations without using divisions that is singularity free?

Let us see: In very general terms, the SHG intensity is proportional to the square of the incoming intensity and the second order electric susceptibility.

$$I_{SHG} \propto \chi^{(2)}_{eff} \chi^{(2)*}_{eff} I_0^2 \tag{5.2}$$

Here, $\chi^{(2)}_{eff}$ denotes the effective second order electric susceptibility of the sample, which determines the SHG intensity. Since it is not possible to determine $\chi^{(2)}_{eff}$ directly, it can only be calculated using the incoming and SHG intensities.

Since we don't know the proportionality constant or the baseline of $\chi^{(2)}$, or the values of the intensities in W/m^2 let us investigate the following expression:

$$\sqrt{\hat{I}_{SHG}} - \hat{I}_0 \tag{5.3}$$

Where the hat denotes that the intensity traces are normalized to their median. If there is no noise in the system and $\chi^{(2)}_{eff}$ is not time dependent, the expression above would evaluate exactly to zero. Then we remember $I_{SHG} \propto \chi^{(2)}_{eff}\chi^{(2)*}_{eff} I_0^2$ from above and simplify:

$$\sqrt{\chi^{(2)}_{eff}\chi^{(2)*}_{eff}\hat{I}_0^2} - \hat{I}_0 = (|\hat{\chi}^{(2)}_{eff}| - 1)\hat{I}_0 \tag{5.4}$$

Let us rewrite the absolute value of the effective, and implicitly normalized (we have normalized both intensity traces to their median) second order susceptibility $|\hat{\chi}^{(2)}_{eff}|$ as a sum of two parts: the first part is constant in time (1) and the second $\Delta\hat{\chi}^{(2)}_{eff}$ is time/potential dependent:

$$|\hat{\chi}^{(2)}_{eff}| = 1 + \Delta\hat{\chi}^{(2)}_{eff} \tag{5.5}$$

Now, we put that in the previous equation and we get:

$$(|\hat{\chi}^{(2)}_{eff}| - 1)\hat{I}_0 = \Delta\hat{\chi}^{(2)}_{eff}\hat{I}_0 \tag{5.6}$$

In short we have calculated:

$$\sqrt{\hat{I}_{SHG}} - \hat{I}_0 = \Delta\hat{\chi}^{(2)}_{eff}\hat{I}_0 \tag{5.7}$$

That is an interesting and very useful result: This way, relative changes in the the effective second order susceptibility can be calculated without the noise ruining the whole party. This way, the situation is much better when compared to $\frac{I_{SHG}}{I_0^2}$. Also we need to remind ourselves that the median of $\hat{I}_0$ is 1 and therefore we can achieve with a reasonable amount of averaging (provided that the fluctuations in $\hat{I}_0$ behave well enough):

$$\overline{\Delta\hat{\chi}^{(2)}_{eff}\hat{I}_0} \approx \Delta\hat{\chi}^{(2)}_{eff} \tag{5.8}$$

5.2 Results

5.2.1 Data Analysis

Several methods were employed to reduce noise as much as possible without "torturing" the data. Finally, I settled for the following procedure:

- take laser intensity data and subtract the measured detector background (2 minutes measurement with all laser beams blocked)
- set the negative values to zero, if they amount to less than 10 percent of the total data points. This is necessary, because the variation in intensity is quite large and as a result of that, some values end up below zero after the mean background is subtracted. The intensity values are integers (detector counts), which exaggerates the problem for very low intensities in my opinion.

- if the share of negative values is too large, the procedure is done after downsampling of the intensity data which is the next step, and this is done to have the same sampling rate in the CV (10 Hz) and the laser data (50 Hz). The downsampling is just taking the average of 5 adjacent points in time.

- take $\sqrt{\hat{I}_{SHG}} - \hat{I}_0$. The reasoning behind this is that the square root compresses the large fluctuation, while the difference provides a kind of pseudo-normalisation to the pulse energy.

- filter this $\Delta\hat{\chi}^{(2)}_{eff}$ in the FFT domain such that only integer multiples of the CV frequency remain. The idea behind this is that, with the potential sweep the system is excited strictly periodically. Therefore, the SHG response has to be strictly periodic too. This means that we have no processes that could alter our system over time significantly, like surface roughening or excessive surface oxidation on the time scale of the CV scan. So we only keep those FFT bins with the right frequencies, that are integer multiples of the CV period. This reduces the noise a lot, as we can discard $N - 1/N$ FFT bins where N is the number of recorded cycles.

- (optional) under the assumption that the noise in the system is mostly white, one can set all the FFT coefficients to zero, where the absolute value crosses a certain threshold (here the median was used). A slightly more advanced version of this is to modify the remaining coefficients like this: $|b_{corr}| = \sqrt{|b|^2 - |b_{med}|^2}$. This assumes that on average the noise is phase shifted by $\frac{\pi}{2}$ relative to the signal, because it is uncorrelated to the signal. Both procedures have a minimal impact on the outcomes.

- take the inverse FFT to go to the time domain again.

- apply a smoothing filter (Savitzky–Golay) to smooth the data. This is necessary, because we kept a lot of FFT coefficients, which correspond to high frequencies. So there is still a lot of high frequency stuff going on. The Savitzky–Golay filtering method dampens these high frequencies. Savitzky–Golay filtering is a standard procedure for peak finding as it preserves the peaks, because it uses information from high frequency components as well. As with most smoothing procedures, there is a trade-off between smoothing and noise reduction.

- average over all cycles without the first and the last one. The first and the last cycle suffer from edge effects from the Savitzky–Golay filter. In addition, the first CV cycle is not stable, as it shows transient behaviour, because it takes a little bit of time for the system to go towards the CV limit cycle (assuming that the sample degradation is slow enough).

5.3 Raw Intensities

The raw intensity data (see Fig. 5.4 and 5.5) are hard to interpret directly due to noise and a decline in intensity. The decline in SHG intensity could be due to sample damage. For example, steel samples or GaN samples are very easy to damage with the focused laser pulses. So it is in some sense quite hard to get meaningful measurements from samples like this without destroying them. But in our case the sample stay intact and the decline in SHG intensity comes only from the decline of the OPG intensity. This can be easily proven by fitting a polynomial to the input intensity (normalized to the median) and comparing its square to a similar fit of the SHG intensity (also normalized). When both line shapes are in good agreement, then the sample is undamaged, because the average $\chi^{(2)}$ is constant (over many cycles).

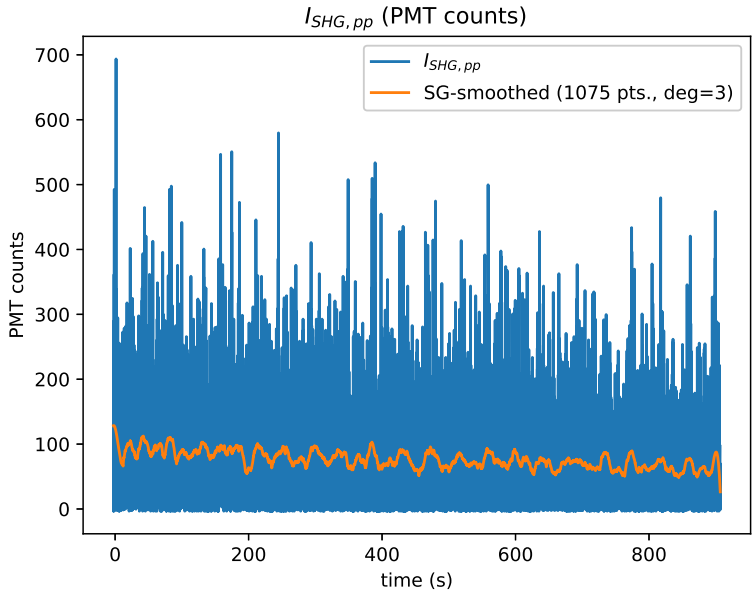

Figure 5.4: SHG detector counts per pulse in pp-polarisation. There is substantial noise and a decline in overall intensity and the smoothed data (1075 points = 21.5 s @ 50 Hz) shows slight oscillations of 43 s which is exactly the CV cycle period

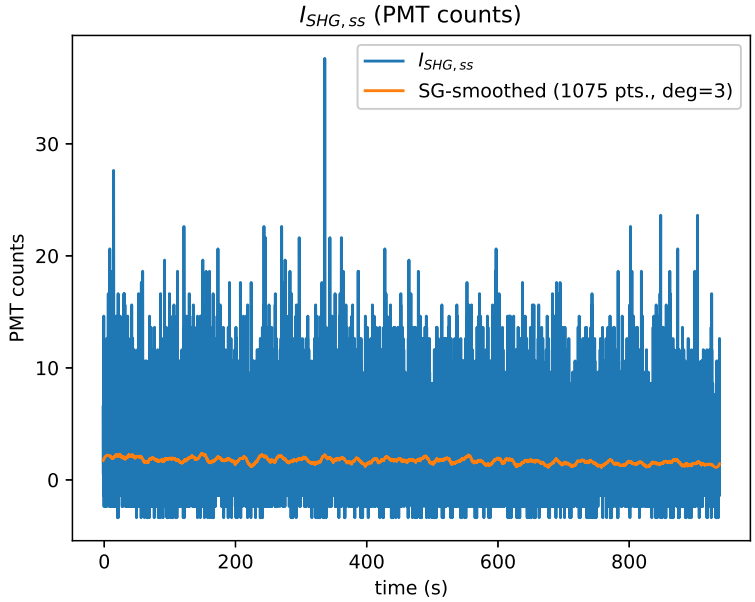

Figure 5.5: SHG detector counts per pulse in ss-polarisation. The mean counts are much much lower. There is also substantial noise and a further delcine in intensity and the smoothed data (1075 points = 21.5 s @ 50 Hz) shows almost no oscillations

5.4 PP-Polarisation

The *pp*-polarisation elicits a stronger overall SH response than the *ss*-polarisation plus the sensitivity to surface changes seems higher than the sensitivity of the *ss*-polarisation.

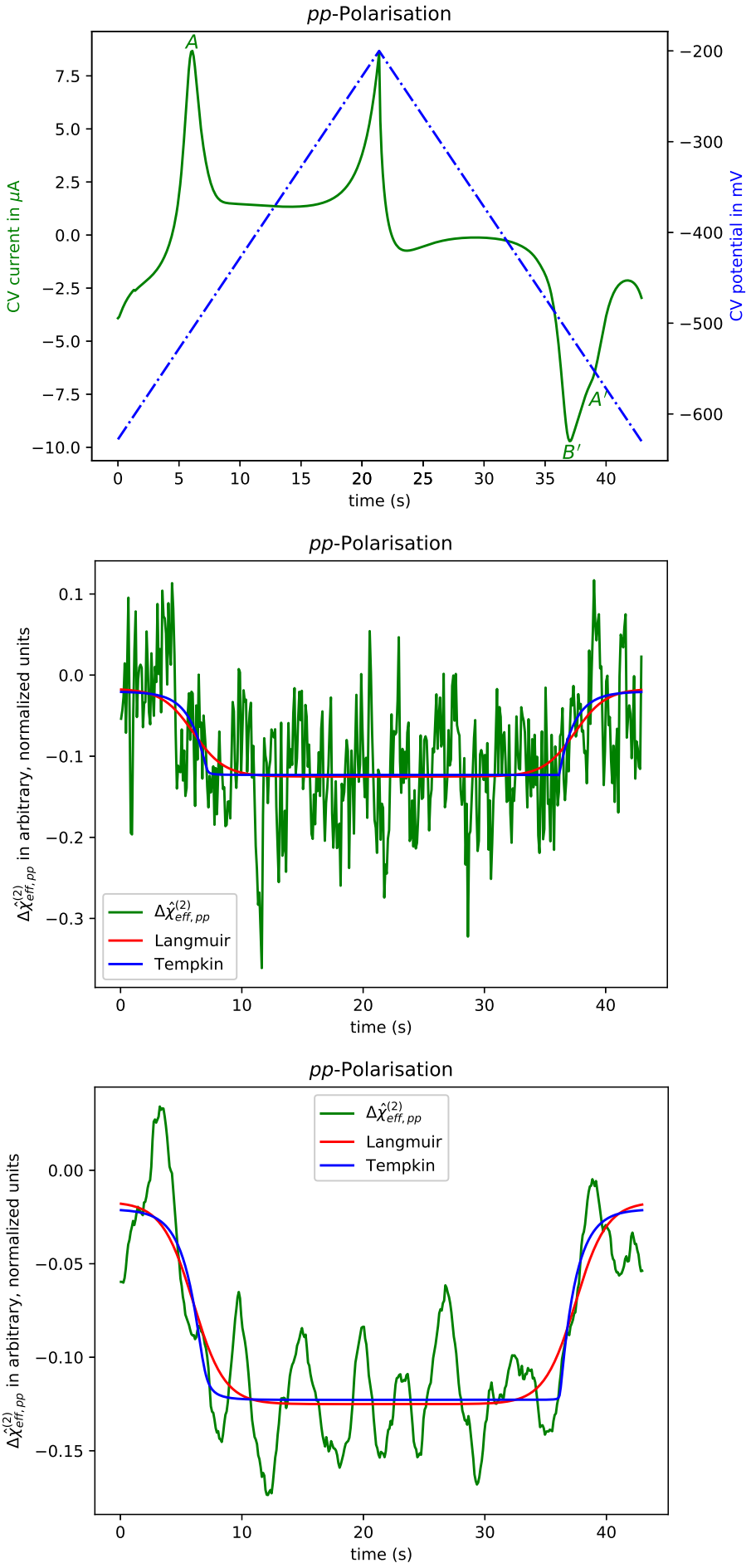

Figure 5.6: **Top:** average CV current (green) and potential (blue) over all cycles without the first one. Current peaks are labelled with A, A' and B'. The period of one cycle is 43 seconds - (continued on the next page)

Figure 5.6: **Center/bottom:** Here, the change in the effective, normalized second order electric susceptibility $\Delta\hat{\chi}^{(2)}_{eff,pp}$, which has been calculated from the intensity data (laser input wavelength: 850 nm) with the line shape of the adsorption isotherms fitted to it in "raw" and smoothed form is shown.

5.4.1 Description of Measurement Data

CV

For the following description of the measurement data see Fig. 5.6. With the CV, a scan speed of 20 mV/s was used. The scan range was from - 630 mV to -200 mV vs. Ag/AgCl in 10 mM HCl. 21 cycles were recorded in total. The scans start at -600 mV in anodic direction (towards 0 mV). At this point the HER (hydrogen evolution reaction) is phasing out and the associated Faraday current diminishes. In this potential region the point of zero charge (PTC) is located (see ref.[3]). This means that the surface has a minimal amount of adsorbed ions. Around 5 seconds and at -550 mV the adsorption of Cl ions starts and results in a peak (A) at 6 seconds. This peak is actually followed by another peak B (see - ref.[3] and ref.[17]), which is small and broad and hard to see in this data. Then the current enters a plateau region from 9-19 s until it rises sharply (exponentially) until the scan direction is reversed at -200 mV or 21.5 s. This type of current is due to the anodic dissolution of copper. The dissolved copper then is redeposited deposited again and causes the current to decrease again and there is a small "bounce" afterwards. The line shape of the current in the HER and the copper dissolution/re-deposition regions can be described with semi-integrals. After that there is a plateau (27-33 s) and two peaks (the larger one at 37 s (B') and a smaller one at 39 s (A')) that are close but can be distinguished visually. These peaks are associated with the desorption of Cl ions and the surface transformations caused by this process. The position of the smaller desorption peak (A') is shifted slightly towards the cathodic direction when compared to the adsorption peak "A. The larger peak (B') is not shifted when compared to peak A. The production of hydrogen (HER) starts at the copper surface (around 40 s, Cl desorption happens at the same time) and increases quasi exponentially, until the scan direction is reversed once more at -630 mV and the HER is phasing out and the starting point is passed again an the cycle starts afresh.

Fits One could fit several peak models and background models to the cyclic voltammogram, which was done by myself. But honestly, this is mainly a good exercise in fitting functions. There is not extremely much of interest one can deduce from fits like that. One can learn that the electron transfer is not reversible, which means the the area under the adsorption and desorption peaks is not the same. Which leads to the question: Where does the peak begin and where does it end?

Optical Data (pp)

The $\Delta\hat{\chi}^{(2)}_{eff,pp}$ (see Fig. 5.6) for the pp-polarisation starts around zero with lots of noise and declines (5-10 s), when the Cl ions adsorb and cause a peak in the CV at the same time. The $\Delta\hat{\chi}^{(2)}_{eff,pp}$ shows a long plateau of reduced SHG efficiency, where the Cl ions are modifying the surface (10-35 seconds). When the Cl ions desorb, $\Delta\hat{\chi}^{(2)}_{eff,pp}$ rises (after 35 s) again simultaneously with the desorption peaks. Some fits of adsorption isotherms to the optial data can be seen in Fig. 5.6. The fit consists of a constant parameter for the background and two adsorption isotherms: one for the adsorption and one for desorption, when the scan goes backwards.

Langmuir Isotherm

Unsmoothed For the anodic scan direction the adsorption (isotherm) is located at -510.0 mV or at *exactly* 6 s. This means that the rate of adsorption is the fastest at this potential, because the Langmuir isotherm is symmetric. Further, this means that the peak of the adsorption current and the position of the (fastest) change in the SHG signal are in exact agreement. The step height of the change in $\Delta\hat{\chi}^{(2)}_{eff,pp}$ is 0.1084, which means a change of 10.8%. For the reverse direction (desorption) the location is of the desorption is -519.1 mV with a step height of 0.1076. This is means that the SHG intensity basically recovers completely (albeit the lock-in FFT filtering method enforces periodicity) and that the desorption is shifted by 9.1 mV (or around 0.5 s) to the cathodic direction. This could be the influence of peak A', which is also shifted into the same direction. The background is: -0.12509.

Smoothed The smoothed data (SG - smoothed over 39 points (=3.9 s @ 10 Hz) - see Fig. 5.6 bottom diagram) gives basically the same parameters: For the anodic scan direction the adsorption (isotherm) is located at -509.9 mV. The step height of the change in $\Delta\hat{\chi}^{(2)}_{eff,pp}$ is 0.1082. For the reverse direction (desorption) the location is of the desorption is -519.0 mV with a step height of 0.1076. The background is: -0.12508.

Tempkin Isotherm The Tempkin isotherm gives similar parameters, but it is not well suited for this data, because the lower limit ($-k_BT$) of the "interaction parameter" w is approached, the linearisation of the exponential yields negative values and fitting is neither useful nor possible. Also, the isotherm features a sharp edge for $w = -k_BT$, which can get "stuck" at distict features in the data. Anyway, w is negative and on the order of 1-2 times ($-k_BT$), which is in line with[19].

Other Isotherms Other isotherms like the Frumkin isotherm are basically impossible to fit to this data, because they are over-parametrized for this job, because the noise masks the exact shape of the isotherm. Also, the fitting has to be done in an implicit manner, which is not easy to do: Origin failed at this and Mathematica too. Then, I wrote some Python functions to do this, which worked well for "nice" test data, with quite some noise added, but failed altogether with the $\Delta\hat{\chi}^{(2)}_{eff,pp}$ data. This problem probably has to do with the residuals, which can get pretty nasty when not treated in a special manner: when data points are fitted which would correspond to a θ that is larger than 1 (due to noise), then the residuals can get large or complex or both and the fit never converges.

5.5 SS-Polarisation

5.5.1 Description of Measurement Data

CV

For the following description of the measurement data see Fig. 5.7. The CV is essentially the same, with slight deterioration of the sample (undesired surface adsorbates like oxygen), as the ss-measurement was recorded after the pp-measurement. This shows as a significant decrease in the peak heights of peak A and B' and some broadening of those peaks.

Optical data (ss)

The *ss*-polarisation (see Fig. 5.7) elicits a much weaker (roughly one order of magnitude) SH response than the *pp*-polarisation. This means, that the recorded counts in the photomultiplier are only a bit above the background noise of the detector. It is rather hard to recognize a clear pattern in $\Delta\hat{\chi}^{(2)}_{eff,ss}$

for the ss-polarisation, but with an excessive amount of smoothing, a gradual decrease from 10-30 s with a sudden increase around 35 s can be seen.

Isotherms The data (see Fig. 5.7) shows no strong correlation with the CV and the fitting of isotherms yields results, that mimic the fitting results for the pp-data in some ways, but those fits cannot be trusted.

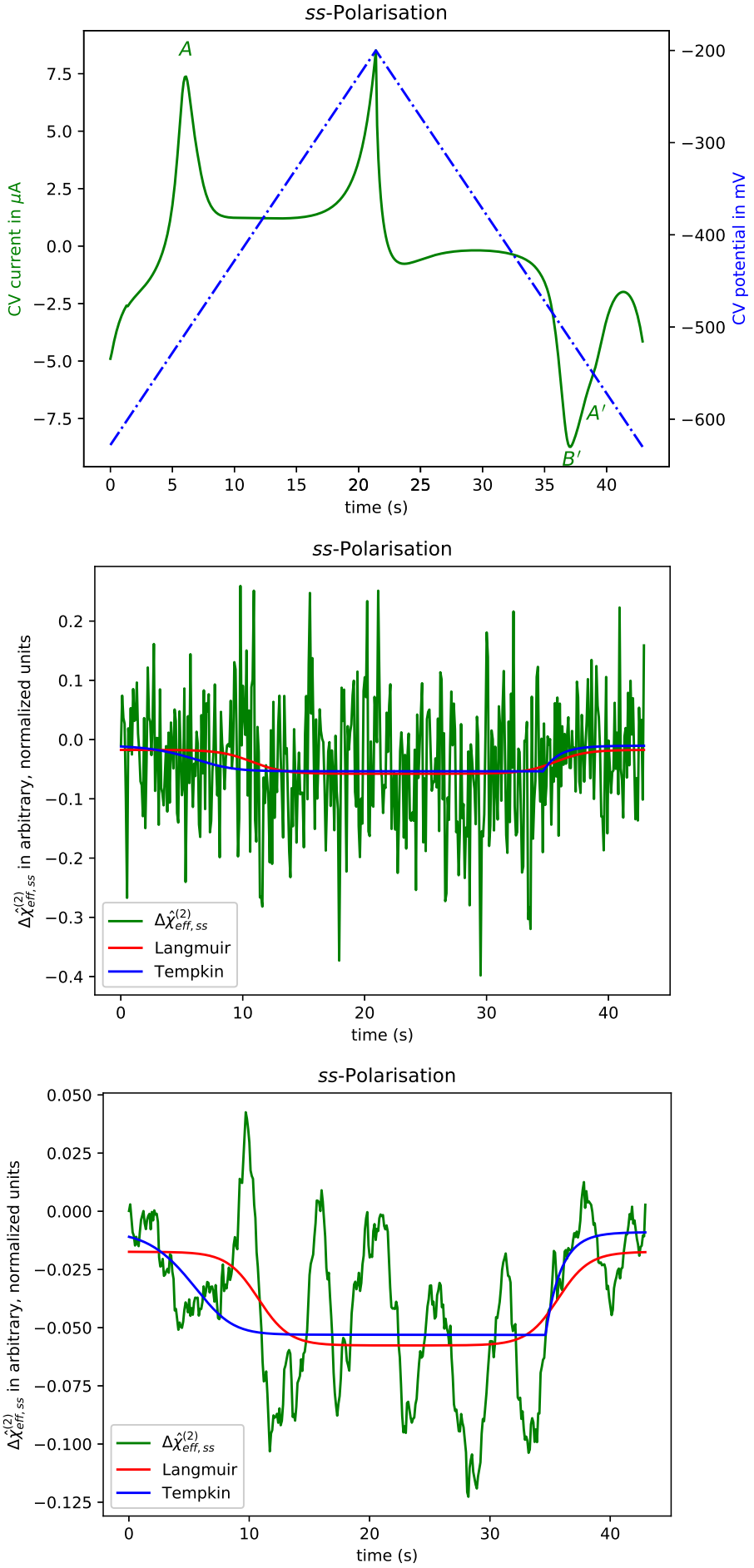

Figure 5.7: Top, center, bottom: average CV current and potential over all cycles without the first one. And $\Delta\hat{\chi}^{(2)}_{eff,ss}$ (laser input wavelength: 850 nm) with the line shape of the adsorption isotherms fitted to it in "raw" and smoothed form

6 Discussion and Further Analysis

6.1 Answers to the Initial Questions

- is there any correlation between CV and SHG and what is a possible mechanism for that?
- can we learn something about the adsorption process itself?
- has CuCl, which forms on the surface at certain potentials a covalent bond between Cu and Cl or is the bond undirected?
- is the electron spillout at the surface homogeneous or not and what does this mean for the SHG intensity/signal at different polarisations?

6.1.1 Correlations

The answer to the first question is: Yes, for the pp-polarisation configuration, there is a clear correlation between CV current and SHG intensity. More specifically, the adsorption peaks in the CV come with *simultaneous* changes in the SHG intensity that look roughly like an integral of the current peaks. Peak A seems to be related to the decrease in $\Delta\hat{\chi}^{(2)}_{eff,pp}$. Similarly, the peaks B' and A' are related to the increase in $\Delta\hat{\chi}^{(2)}_{eff,pp}$. Which one of the two peaks is responsible for the change? Sadly, this cannot be deduced with the data at hand. Anyway, a change in surface coverage gives rise to a current, that is associated with the necessary sorption processes and associated surface transformations. And those changes so it seems, lead to a change in the second order electric susceptibility of the surface and therefore the the SHG intensity changes too.

6.1.2 Possible Mechanisms

Now comes the second and harder part of the first question: What kind of mechanism is responsible for the change in SHG intensity, when adsorption and desorption occurs at the surface of the Cu(110) sample? I suspect, that without advanced calculations or even some simulations, this question cannot be answered sufficiently well. But lets take a guess: The change in surface charge distorts the rim of the effective potential at the surface for the electrons (where the surface dipole of a metal sits). This changes the "abruptness" of the transition from the surface to the bulk of the metal. Since an appreciable surface SHG response depends strongly on the presence of a rather sharp discontinuity, changes of the surface influence the SHG signal.

This would explain the pp-polarisation measurements at least superficially. But what is with the ss-polarisation? As described earlier, from the symmetry of an ideal Cu(110) surface it should follow, that there is no SHG signal (at least in the el. dipole approximation). There are several additional caveats: the crystallographic orientation of the sample (accuracy of alignment/cutting of the single crystal) is guaranteed only to 1° accuracy by the manufacturer and the polishing process (done per hand with a simple machine) could have made this a bit worse. Further, the polarisation directions of the half wave plate and the analyser prisms have markings only every two degrees, and the half

wave plate has to be placed per hand in the housing, and has no convenient notch for alignment (but markings).

The ss-polarisation is much weaker in SHG intensity than pp-polarisation, but it is not zero either. This may point to a hydrodynamical model of SHG, where covalent bonds play not much of a role. In 3.6.3, the parallel surface currents, which would contribute to a SHG response in the ss-configuration are treated. Another possibility could be that the rectangular symmetry is broken globally, which could be an effect as simple as a slightly slanted surface which would introduce steps, that would break the rectangular symmetry of the surface.

Maybe we can learn something from the expressions, which we obtained from our SBHM calculations in 3.7 and especially equ. 3.55:

$$|\chi_2| \simeq 7|\gamma_{Cu}| + 4|\gamma_{CuCl}| \cos(\phi)\, \theta \tag{6.1}$$

Below, the vertical bars for the absolute values of the hyperpolarizabilities have been omitted. For $\theta = 0, 1$ we get:

$$|\chi_2| \simeq 7\gamma_{Cu} \qquad \text{and} \qquad |\chi_2| \simeq 7\gamma_{Cu} + 4\gamma_{CuCl} \cos(\phi) \tag{6.2}$$

We then look to the measurement results and fits for the pp-polarisation (see 5.4.1) and set:

$$|\chi_2| \simeq 7\gamma_{Cu} \approx 1 \qquad \text{no Cl adsorbed} \qquad \theta = 0 \tag{6.3}$$

and

$$|\chi_2| \simeq 7\gamma_{Cu} + 4\gamma_{CuCl} \cos(\phi) \approx 0.9 \qquad \text{Cl adsorbed} \qquad \theta = 1 \tag{6.4}$$

with that we can calculate:

$$\gamma_{Cu} = \frac{1}{7} \qquad \text{and} \qquad \gamma_{CuCl} \cos(\phi) = -\frac{-1}{40} \tag{6.5}$$

Since the absolute (unnormalized) value of both hyperpolarizabilities cannot be determined, we look at their ratio:

$$\frac{\gamma_{Cu}}{\gamma_{CuCl} |\cos(\phi)|} = \frac{40}{7} \approx 5.7 \tag{6.6}$$

We cannot obtain the hyperpolarizabilities or their ratio directly due to $\cos(\phi)$, which is at least slightly negative and therefore adsorption diminishes the SHG intensity. Which of the two multipliers is responsible for the small value of $\gamma_{CuCl} |\cos(\phi)|$ is not clear. Also we may overestimate γ_{Cu}, because every possible mechanism (free electrons...) that contributes to the background is included there. The SBHM works better if measurement data is available where the sample is rotated around its surface normal.

6.1.3 Adsorption

What about the adsorption process? Adsorption clearly changes SHG response. Regrettably, the data for the pp-polarisation is not good enough to distinguish between Langmuir and other isotherms. But at least it does not contradict the Langmuir and Tempkin isotherms. For the Frumkin isotherm, the data is too bad to do any fit at all. I tried several programs to fit it, but it does not converge even with a hand-tuned, self written python method for implicit fitting, which works for fairly nice test data. For this measurement data the Frumkin isotherm has probably one parameter too much.

6.1.4 CuCl-Bond

What about the bond of CuCl? Covalent or more ionic? And in which direction does it point? This can determined hopefully with experiments in which the sample is rotated around its surface normal. Additional surface SFG measurements could help.

6.1.5 Electron Spillout

From the data, there is not a lot, that can be said. But my guess is that the electrons spill out in a manner that shows the atomic structure/arrangement of the surface (That's why (EC-)STM works). Does this influence the SHG signal (ss-polarisation)? From a symmetry perspective, rather not, but from the hydrodynamical equations maybe yes.

6.2 Further Discussion

There are several things, that need some further discussion or further mention:

- Surface SHG is *quite* surface sensitive when compared to RAS or ellipsometry in the system under study. For the pp-polarisation, $\Delta\hat{\chi}^{(2)}_{eff,pp}$ decreases around 10 percent, which is orders of magnitude more than with RAS or ellipsometry. This is a great advantage, because the measurement results are more "stable" in the sense that small perturbations of the experimental setup do not destroy an experiment immediately. The (in principle rather high) sensitivity could enable close monitoring of the adsorption processes or maybe reveal 2D-phase transitions of surface adsorbates (island formation).
- RAS and ellipsometry could benefit from using FFT filtering for post-processing the optical measurement data (Only for cyclic processes). This would enhance the signal to noise ratio a lot and it is easy to implement and fast to compute, when the data is available as a time series.
- Cl adsorption diminishes the SHG efficiency, while copper dissolution or hydrogen evolution seems to have no major effect. This is very similar to the RAS measurements which where performed at ZONA in the past.[19]. The RAS data are much better, even tough the RAS sensitivity is 2 orders of magnitude lower.
- sample deterioration/oxidation kills the sensitivity (change in SHG intensity) to adsorption quite fast. This comes with a decrease in the height of the adsorption peaks and some broadening of those peaks.
- the ss-polarisation might be influenced by peaks B and surface scattering/faceting, which needs more measurements to confirm this hypothesis.

6.3 Conclusion and Outlook

It seems that the Cl adsorption diminishes the SHG efficiency. In the free electron model discussed in the theory part, the change stems from a change in the electronic surface charge, which is caused by the electrostatic repulsion by the Cl ions.

But the change could come from basically anything, that is influenced by the Cl sorption processes. For example from the electrolyte side of the interface (EFISH, ordering effects of water) or a Cl-copper "bond" for example.

In principle, the sensitivity is not bad and could be used to determine the surface charge, provided, that the noise in the system can be managed. To monitor the surface charge accurately, some reference point (measured with a non- optical method) is probably needed to calibrate the optical measurements. To further test this theories, more experiments are needed.

6.3.1 Outlook

There are several ways, in which this measurements can (and will be) improved upon:

- more cycles and slightly slower scan speed, to increase the resolution of the "peaks" and to suppress noise
- better sample preparation (and sample holder) to get clearer peaks in the cyclic voltammogram
- using 532 nm as wavelength from the H500: the pulses are much more intense and much less noisy. Plus, copper has a stronger SHG response at this wavelength for both s- and p-polarized input radiation (see ref.[9]) due to the interband transitions in this wavelength region.
- a rotatable cell to probe surface symmetry (tricky) or even SFG (can be used to probe surface symmetry by switching up polarisations).
- better cooling system that uses a PID controller instead of a bang-bang controller.

Bibliography

[1] J Bard Allen and R Faulkner Larry. *Electrochemical methods fundamentals and applications*. John Wiley & Sons, 2001.

[2] Nicolaas Bloembergen, Richard K Chang, SS Jha, and CH Lee. Optical second-harmonic generation in reflection from media with inversion symmetry. *Physical Review*, 174(3):813, 1968.

[3] Miao-Hsuan Chien, Saul Vazquez-Miranda, Reza Sharif, Kurt Hingerl, and Christoph Cobet. In Situ Optical Quantification of Adsorbates and Surface Charges on Copper Crystals and Their Impact on the Hydrogen Evolution Reaction in Hydrochloric Electrolytes. *The Journal of Physical Chemistry C*, 122(16):8984–8997, 2018.

[4] P Guyot-Sionnest, W Chen, and YR Shen. General considerations on optical second-harmonic generation from surfaces and interfaces. *Physical Review B*, 33(12):8254, 1986.

[5] H. C. Hamann. *Electrochemistry*. Wiley-VCH, 2000.

[6] John David Jackson. *Classical electrodynamics*. Wiley, New York, NY, 3rd ed. edition, 1999.

[7] Jerome Spanier Keith B. Oldham. *The Fractional Calculus: Theory and Applications of Differentiation and Integration to Arbitrary Order*. Dover Books on Mathematics. Dover Publications, 2006.

[8] Florian Maurer, Joachim Brötz, Shafqat Karim, Maria Eugenia Toimil Molares, Christina Trautmann, and Hartmut Fuess. Preferred growth orientation of metallic fcc nanowires under direct and alternating electrodeposition conditions. *Nanotechnology*, 18(13):135709, 2007.

[9] G Petrocelli, S Martellucci, and R Francini. Wavelength dependence of second-harmonic generation at the copper surface. *Applied Physics A*, 56(3):263–266, 1993.

[10] G Petrocelli, S Martellucci, F Scudieri, and A Agostini. Second-harmonic generation at the Al and Cu surfaces for the fundamental wavelength of λ= 532 nm. *Applied physics letters*, 59(20):2501–2503, 1991.

[11] Richard C Powell. *Symmetry, Group Theory, and the Physical Properties of Crystals*. Springer-Verlag New York, 2010.

[12] Marvin Radke. Stern Modell. `https://commons.wikimedia.org/wiki/File:Stern_Modell.png`, 20. November 2016. [Online; accessed Wednesday 18th November, 2020].

[13] Adam Redzikowski. Three electrode setup. `https://commons.wikimedia.org/wiki/File:Three_electrode_setup.svg`, 11 February 2013. [Online; accessed Wednesday 18th November, 2020].

[14] Cornelia Reitböck, David Stifter, Adalberto Alejo-Molina, Hendradi Hardhienata, and Kurt Hingerl. Nonlinear ellipsometry of Si (111) by second harmonic generation. *Applied Surface Science*, 421:761–765, 2017.

[15] Cornelia Reitböck, David Stifter, Adalberto Alejo-Molina, Kurt Hingerl, and Hendradi Hardhienata. Bulk quadrupole and interface dipole contribution for second harmonic generation in Si (111). *Journal of optics*, 18(3):035501, 2016.

[16] Joseph Rudnick and E.A. Stern. Second-harmonic radiation from metal surfaces. *Physical Review B*, 4(12):4274, 1971.

[17] Gholamreza Barati Sedeh. *Electrochemical Scanning Tunneling Microscopy of Cu(110) in Chloride Containing Solutions.* Dissertation, Johannes Kepler Universität Linz, Zentrum für Oberflächen und Nanoanalytik, 2015. `http://epub.jku.at/obvulihs/content/titleinfo/417045`.

[18] YR Shen. Surface Second Harmonic Generation: A New Technique for Surface Studies. *Annual Review of Materials Science*, 16(1):69–86, 1986.

[19] Saul Vazquez-Miranda, Vladyslav Solokha, Raul E Balderas-Navarro, Kurt Hingerl, and Christoph Cobet. Adsorbate isotherm analysis by reflection anisotropy spectroscopy on copper (110) in hydrochloric acid. *The Journal of Physical Chemistry C*, 124(9):5204–5212, 2020.

Eidesstattliche Erklärung

Ich erkläre an Eides statt, dass ich die vorliegende Masterarbeit selbstständig und ohne fremde Hilfe verfasst, andere als die angegebenen Quellen und Hilfsmittel nicht benutzt bzw. die wörtlich oder sinngemäß entnommenen Stellen als solche kenntlich gemacht habe. Die vorliegende Masterarbeit ist mit dem elektronisch übermittelten Textdokument identisch.

Linz, am 18.11.2020

Josef Resl BSc